UNIVERSITY OF CALIFORNIA

Los Angeles

CFD-based skirt baffle depth optimization for secondary sedimentation tank

A thesis submitted in partial satisfaction

of the requirements for the degree Master of Science in

Civil Engineering

by

Yuyang Zhou

2023

ABSTRACT OF THE THESIS

CFD-based skirt baffle depth optimization

for secondary sedimentation tank

by

Yuyang Zhou

Master of Science in Civil Engineering

University of California, Los Angeles, 2023

Distinguished professor Michael K. Stenstrom, Chair

Computational fluid mechanics were used to determine the optimal depth of a skirt baffle in a circular-type secondary clarifier. Three sets of simulations were performed. The first, set A, determined the better range of operation conditions; set B investigated the numerical stability of the simulations and served as a base for simulation and set C which analyzed the skirt baffle depth on the effluent suspended solids, recycle solids concentration and biosolids mass in the clarifier. The skirt baffle depth was evaluated for three sets of surface overflow conditions and ranged from 10% to 90% of the clarifier depth. Best clarifier performance occurred when the skirt baffle depth was approximately 70% of the clarifier depth. The analysis used Fluent® log files to create a less time-consuming approach for clarifier analysis.

The thesis of Yuyang Zhou is approved.

Jennifer A. Jay

Sanjay K. Mohanty

Michael K. Stenstrom, Chair

University of California, Los Angeles

2023

Index

List of Figures

List of Tables

Nomenclature

SS= Suspended solid

TSS= Total suspended solids

MLSS= Mixed liquor suspended solids

SST= Secondary sedimentation tank

WWTP= Wastewater treatment plant

EDI= Energy dissipated inlet

RAS= Returned activated sludge

ESS= Effluent suspended solids

SBH= Sludge blanket height

SOR= Surface overflow rate

SLR= Solid loading rate

Depth ratio= Baffle depth / total depth from surface to the bottom

RAS ratio= RAS flow rate / Influent flow rate

SKE= Standard k-ε model

CFD= Computational fluid dynamics

DNS= Direct Numerical Simulation

RANS= Reynolds Averaged Navier-Stokes

URANS= Unsteady Reynolds Averaged Navier-Stokes

LES= Large Eddy Simulation

Acknowledgements

I would like to extend my sincere gratitude to my adviser, Distinguished Professor Michael K. Stenstrom, for his advice and assistance in the preparation of my thesis. I am really impressed by the degree of knowledge and skill that Distinguished Professor Michael K. Stenstrom has demonstrated to me during my studies.

I would especially want to thank Dr. Haiwen Gao for sharing his invaluable knowledge in CFD simulation of SST with me.

I would like to thank the rest of my thesis committee, Professor Jennifer Jay, and Associate Professor Sanjay Mohanty. I am grateful for the suggestions and modifications the committee made in this thesis.

I would like to thank my parents, Jikai Zhou, and Hui Li, for their love and support, especially during my MS studies at UCLA.

1 Introduction

1.1 Background

Ever since the invention of the activated sludge process (Ardern & Lockett, 1914), separating suspended solids from the effluent of bioreactor remains the primary issue for improving the quality of wastewater treatment plants (WWTPs) effluent. Secondary settling tanks are the most common way to remove suspended solids from bioreactor effluent. The performance of secondary settling tanks relies on numerous processes such as turbulence, sludge rheology, hydrodynamics, etc. (McCorquodale, 2004).

The vertical baffle in the middle of the SST has considerable influence on SST performance. It has several different names, such as skirt baffle, center well, stilling well, etc. In this thesis, it will be called skirt baffle. Along with the Energy Dissimating Inlet, the skirt baffle is designed to reduce the turbulence impact of the inlet flow. Once an SST is built, it is hard to change its solid structure like diameter and depth. However, better performance can be achieved by changing the depth of the skirt baffle at less cost.

1.2 Objectives

With the aid of CFD modeling, numerical experiments can be carried out with less time and cost. Most previous research projects only focused on complex cases and are limited to a small range of operating conditions due to the extremely long time required for simulations. In this study, in order to find a less time-consuming way for SST structure optimization, a series of simulations were conducted with simple 2D geometry. The influence of skirt baffle depth on SST performance was tested. It was also necessary to evaluate the stability of CFD simulations. Finally, an optimal baffle depth ratio of the given geometry was determined.

2 Literature Review

2.1 CFD in Clarifiers Design

2.1.1 1-D flux theory

The research concerning sedimentation can be trace back to early 20th century. Hazen (1904) introduced surface overflow rate (SOR) into the design of settling tanks. SOR and solids loading rate (SLR) are still two crucial criteria used to determine whether the design is logical till now.1-D flux theory originated from solid flux theory (Kynch, 1952). Solid flux theory assumed that gravity settling velocity only relates to suspend solid concentration. Bryant (1972) developed the first 1-D flux model for continuous thickening. However, the limiting flux can be exceeded in that model. Stenstrom (1976) applied it to clarification-thickening process and modified it by adding flux constraint. The constraint required gravity flux in one layer not to exceed that in next one. Vitasovic (1986) developed a full-scale SST dynamic model. He added another layer above the feed point to simulate the upwelling current. 1-D flux theory ignores hydrodynamic complexities of an actual settling tank and leading an overdesigned SST.

2.1.2 2D or 2Dc models

The first 2D clarifier modeling was presented by Larsen (1977). 2D models aimed to solve the 2D hydrodynamic field through CFD. After that, McCorquodale (2004) developed a Fortran-based Quasi 3-D non-steady state secondary settling tank. Gao (2016) performed several simulations using the 2Dc (Quasi 3D) model McCorquodale developed to verify the data from previous literature (Vitasovic et al., 1997) and analyze the influential factors for secondary clarifiers. Gao and Stenstrom (2020a) with ANSYS fluent 2D investigated the influence of

different turbulence models on predicting the steady-state hydrodynamics of a secondary sedimentation tank.

Due to the lack of computing power, most models developed before 2000 were 2D or 2Dc models. 2D or 2Dc models have a considerable improvement in simulating actual SST compared to the 1-D flux theory. However, most of the models describing circular SSTs are based on axisymmetric assumption, ignoring the fact that most existing circular SSTs are asymmetric, which leads to an inaccuracy in simulation.

2.1.3 3D simulations

3D simulations have been undergoing rapid growth in the past decade benefiting from the exponential growth of computing power. 3D simulations are too complex to code independently, so nearly all simulations are based on a CFD software package. ANSYS Fluent (Lainé et al., 1999) and PHOENICS (Dahl et al., 1994) are two of the most popular commercial software for SST simulations. OpenFOAM is an opensource software which is less utilized but is still a desirable choice for some complex issues requiring coding.

3D simulations enable researchers to investigate some more realistic factors such as wind, EDI performance, etc. For example, with the aid of ANSYS Fluent 3D, Gao and Stenstrom (2020b) investigated the effects of wind on circular SST performance. They found that the circular SST clarification performance is very sensitive to the wind.

2.2 Fluid Dynamic and its Application to SST Design

2.2.1 Lagrangian and Eulerian Description

Lagrangian and Eulerian are the two ways used to describe fluid motion. In the Lagrangian description, a single fluid parcel is tracked over time and space. The Eulerian description, on the other hand, focuses on particular place in the space through which the fluid moves as time passes (Batchelor, 1973). The Lagrangian description is more suitable for discrete particles simulation, but it requires more computation power. The Eulerian description is more suitable for fluid description but may result in numerical instability. Most single-phase models are based on Eulerian description. The Lagrangian description is becoming more popular in recent years due to the increase in computation power.

2.2.2 Turbulence Models

Turbulence is the most important characteristic of fluid. And it is one of the major factors influencing the performance of SST (Dobbins, 1944). There are three major turbulence models, Direct Numerical Simulation (DNS), Large eddy simulation (LES), and Reynolds Averaged Navier-Stokes (RANS). DNS is calculated by directly solving the N-S equations. The computation resources required are considerably high. The LES ignores small turbulence and uses only the larger turbulence by DNS. It has less computational cost compared to DNS and has developed rapidly in recent years. The most popular and widely used method in industrial applications is RANS. RANS derives equations by averaging over time. RANS equations are very similar to the original N-S equations but include some additional terms known as Reynolds stress terms. Reynolds stress terms require k (turbulent kinetic energy) and ε (dissipation rate of turbulent kinetic energy) to solve. Based on the ways to solve k and ε, three major RANS models have been developed, SKE, RNG k-ε, and Realizable k-ε. Gao and Stenstrom (2018) evaluated

three RANS models, and found that turbulence model selection can have a strong influence on the prediction of flow capacity. Traditional RANS is limited to steady situations. So unsteady RANS (URANS) was developed to resolve dynamic flows.

2.2.3 Multiphase Models

Multiphase models are widely used in Environmental Engineering, dealing with many pollutants transportation process including sedimentation process. There are two major approaches of multiphase models, Euler-Lagrange and Euler- Euler (Brennen & Brennen, 2005). The Euler-Lagrange model calculates liquid phase using the Eulerian description while the solid phase is calculated using the Lagrangian description. In this case, the solid phase fraction is assumed to have much less mass than fluid phase. It is more commonly used to simulate sediment transport in channels. In the Euler- Euler approach, phases are assumed to be able to overlap with each other. The volume fractions are introduced in coupled phases. The sum of the volume fractions over all phases should be equal to one. There are two major Euler- Euler models, VOF model, and Mixture model. The VOF model tracks the surface between two or more immiscible fluids, while the Mixture model solves for the mixture momentum equation.

2.3 Settling Mechanism

Settling of suspend solid can be divided in to four different types: Type I - Discrete settling, Type II - Flocculent settling, Type III - Zone or hindered settling, and Type IV - Compression settling (Ekama et al., 1997). In the discrete settling stage, which often occurs at high turbulence regime, there is no apparent flocculation. The particle follows Stokes' law. In flocculent settling stage, flocculation is the dominate process. Malcherek (1994) presented a power model including average velocity gradient to describe the settling speed in this stage. In the zone or hindered settling stage, the concentration of particles or sludge is relatively high.

High concentration sludge starts to exhibit the properties of a non-Newtonian fluid. The settling velocity description is quite different from previous stages. Vesilind's equation was proved to be the best prediction of zone settling velocity (Vesilind, 1968). In compression settling stage, the water ratio in the sludge decreases rapidly and induces a change in floc structure. The compression settling is viewed as an extension of zone settling. Vesilind's expression is still applicable in this stage.

There are also some combined models that aim to describe all settling stages in one formula. The most widely used combined model was proposed by Takács et al. (1991). Numerous CFD simulations were carried out with the aid of Takács model (De Clercq, 2004; Gao & Stenstrom, 2018; Lakehal et al., 1999; McCorquodale, 2004; Vitasovic et al., 1997).

2.4 Baffle Structures

Inlet structures can be divided into energy dissipating inlets (EDI) and some baffle structures such as McKinney baffle and skirt baffle. The Inlet structures have been proven to be one of the major factors influencing SST performance (Tekippe, 2002). One of the most popular EDI designs is tangential EDI with four to eight openings. The LA-EDI is a new design implemented at the Los Angeles-Hyperion plant. It is reported to have increased the capacity of the existing clarifiers by more than 50 percent (Haug et al., 1999).

The Mc Kinney baffle is a horizontal baffle below the inlet ports. Trials in the Witney WWTP showed tank with a McKinney baffle generates a lower ESS than one without a McKinney baffle at an equivalent flow rate (Burt, 2010). The Skirt baffle is a vertical baffle in the middle of the tank diameter. Vitasovic et al. (1997) reduced the size of the skirt baffle from 46% to 28% of the tank diameter in their simulation and found an 80% decrease in ESS.

The Stamford baffle is the most common outlet structure in existing WWTPs. Stamford baffle is an inclined baffle near the outlet. Gerges and McCorquodale (2008) found that the Stamford baffle with a 60-degree angle has a better performance than traditional 45-degree angle ones.

3 Material and Methods

3.1 Geometry and Meshing

The geometry of this study is adapted from the SSTs in Darvill WWTP (Ekama and Marais, 2002). The 2D axisymmetric geometry of the SST is shown in Figure 3.1. The Darvill tanks have a diameter of 35m and a depth of 5.7m. Its bottom slope is 10% and the sludge is scraped to the center bottom outlet.

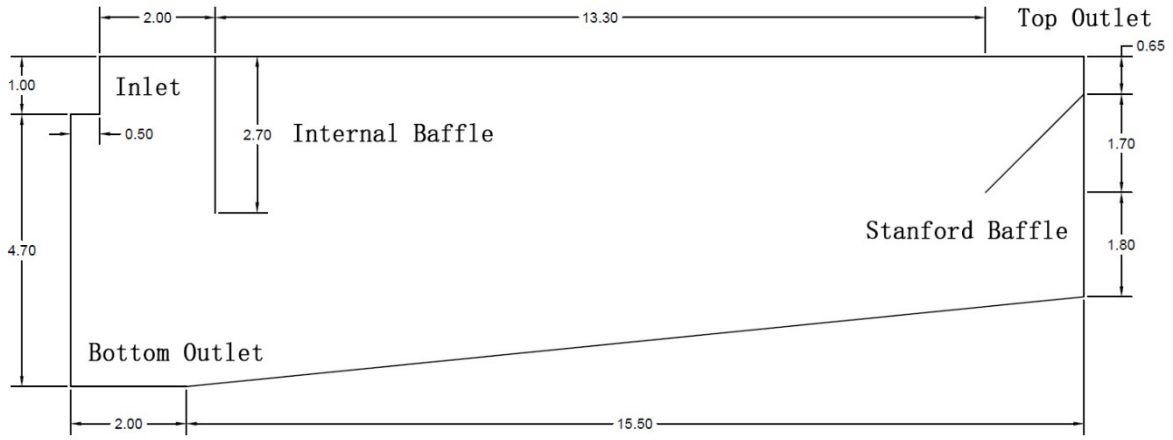

Figure 3.1 Geometry of the Darvill SST

The grid is generated by ANSYS-ICEM as a structured grid. Structured grids have an advantage over unstructured grids in that they have a much better grid quality. The grid boundary layer is thickened to improve calculating quality. Two grids with 218,700 and 115,620 cells were tested for grid independence. The size of 115620 is sufficient for a grid-independent result.

The simulation was then carried out using ANSYS-Fluent with UDF (user-defined functions). The CPU used is AMD R9 5900HX eight-core processor. All simulations are set to steady and axisymmetric. Each simulation has 50,000 iterations and is computed on one core. Each simulation consumes about 1 hour of computing time. Increasing cores used for simulation

will not decrease the time needed significantly. That might be because the grid size is too small for parallel computing.

3.2 Governing Equations

The following equations derived from Navier- Stokes equations for incompressible fluids describe the basic hydrodynamics of cylindrical SST in 2D axisymmetric conditions (Ekama et al., 1997):

Continuity equation:

$$\frac{\partial ru}{\partial r} + \frac{\partial rv}{\partial y} = 0 \tag{1}$$

Momentum equation – Angular:

$$\frac{\partial u}{\partial t} + u\frac{\partial u}{\partial r} + v\frac{\partial u}{\partial y} = -\frac{l}{\rho}\frac{\partial p}{\partial r} + \frac{l}{r\,\partial r}\left(rv_t\frac{\partial u}{\partial r}\right) + \frac{l}{r}\frac{\partial}{\partial y}\left(rv_t\frac{\partial u}{\partial y}\right) + S_u \tag{2}$$

$$S_u = \frac{l}{r}\frac{\partial}{\partial r}\left(rv_t\frac{\partial u}{\partial r}\right) + \frac{l}{r}\frac{\partial}{\partial y}\left(rv_t\frac{\partial v}{\partial r}\right) - 2\frac{v_t}{r^2}u \tag{3}$$

Momentum equation – Vertical:

$$\frac{\partial v}{\partial t} + u\frac{\partial v}{\partial r} + v\frac{\partial v}{\partial y} = -\frac{1}{\rho}\frac{\partial p}{\partial y} + \frac{1}{r}\frac{\partial}{\partial r}\left(rv_t\frac{\partial v}{\partial r}\right) + \frac{1}{r}\frac{\partial}{\partial y}\left(rv_t\frac{\partial v}{\partial y}\right) + g\frac{\rho-\rho_r}{\rho} + S_v \tag{4}$$

$$S_v = \frac{l}{r}\frac{\partial}{\partial r}\left(rv_t\frac{\partial u}{\partial y}\right) + \frac{1}{r}\frac{\partial}{\partial y}\left(rv_t\frac{\partial v}{\partial y}\right) \tag{5}$$

where u and v are velocity in r (angular) and y (vertical) directions respectively; ρ is the fluid density; p is the pressure at reference density ρ_r; v_t is eddy viscosity; g is the gravitational acceleration and $g\frac{\rho-\rho_r}{\rho}$ is the density gradients term added to the Navier- Stokes equations.

The turbulence model used in this study is RANS (Reynolds-averaged Navier–Stokes) with SKE (standard k-ε model). This model is a built-in function of ANSYS- Fluent. A brief overview of the equations follows:

Reynolds-averaged Navier–Stokes equation:

$$\rho\bar{u}_j\frac{\partial\bar{u}_i}{\partial x_j}=\rho\bar{f}_i+\frac{\partial}{\partial x_j}\left[-\bar{p}\delta_{ij}+\mu\left(\frac{\partial\bar{u}_i}{\partial x_j}+\frac{\partial\bar{u}_j}{\partial x_i}\right)-\rho\overline{u_i'u_j'}\right] \tag{6}$$

Boussinesq eddy viscosity assumption is proposed to solve the inner product term $-\rho\overline{u_i'u_j'}$:

$$-\rho\overline{u_i'u_j'}=\mu_t\left(\frac{\partial U_i}{\partial x_j}+\frac{\partial U_j}{\partial x_i}-\frac{2}{3}\frac{\partial U_k}{\partial x_k}\delta_{ij}\right)-\frac{2}{3}\rho k\delta_{ij} \tag{7}$$

$$\mu_t=\rho C_\mu\frac{k^2}{\varepsilon} \tag{8}$$

where μ_t is eddy viscosity. To obtain the eddy viscosity, k and ε are needed. In SKE model, k and ε are calculated using following equations:

Turbulent kinetic energy k equation:

$$\frac{\partial(\rho k)}{\partial t}+\frac{\partial(\rho k u_i)}{\partial x_i}=\frac{\partial}{\partial x_j}\left[\frac{\mu_t}{\sigma_k}\frac{\partial k}{\partial x_j}\right]+2\mu_t E_{ij}E_{ij}-\rho\varepsilon \tag{6}$$

Dissipation ε equation:

$$\frac{\partial(\rho\varepsilon)}{\partial t}+\frac{\partial(\rho\varepsilon u_i)}{\partial x_i}=\frac{\partial}{\partial x_j}\left[\frac{\mu_t}{\sigma_\varepsilon}\frac{\partial\varepsilon}{\partial x_j}\right]+C_{1\varepsilon}\frac{\varepsilon}{k}2\mu_t E_{ij}E_{ij}-C_{2\varepsilon}\rho\frac{\varepsilon^2}{k} \tag{7}$$

where u_i represents velocity component in corresponding direction; E_{ij} represents component of rate of deformation; μ_t represents eddy viscosity; Adjustable constants values are suggested as follows: $C_\mu=0.09$, $\sigma_k=1.00$, $\sigma_\varepsilon=1.30$, $C_{1\varepsilon}=1.44$, $C_{2\varepsilon}=1.92$.

To simulate the transport of sludge, the conservation equation and sludge property equations are needed. They are shown as follows:

Conservation of concentration equation:

$$\frac{\partial X}{\partial t} + u\frac{\partial X}{\partial r} + v\frac{\partial X}{\partial y} = \frac{1}{r}\frac{\partial}{\partial r}\left(rv_{sr}\frac{\partial X}{\partial r}\right) + \frac{1}{r}\frac{\partial}{\partial y}\left(rv_{sy}\frac{\partial X}{\partial y} + rV_s X\right) \tag{7}$$

where X is concentration of SS; v_{sr} is the eddy diffusivity of suspended solids in the r direction; v_{sy} is the eddy diffusivity of suspended solids in the y direction; and V_s is particle settling velocity.

The sludge settling velocity equation (Takács et al., 1991) is:

$$u_{sj} = Min(u_0 e^{-r_h x_j^*} - u_0 e^{-r_p x_j^*}, u_0), \quad u_{sj} \geq 0 \tag{8}$$

where u_{sj} is sludge settling velocity; u_0 is Stokes velocity; x_j^* is calculated by the SS concentration x minus non-settleable SS concentration x_{min}; r_p represents the settling parameter for rapidly settling floc; and r_h represents the settling parameter for poorly settling floc.

The sludge viscosity equation (Bokil, 1972) is:

$$v = \begin{cases} -1 \times 10^{-6} e^{1.386C} & C \leq 1\text{g/L} \\ 2.9 \times 10^{-6} e^{0.322C} & C \geq 1\text{g/L} \end{cases} \tag{9}$$

where v is the plastic viscosity of the sludge; and C is the concentration of suspend solid.

3.3 Model Verification

The model is verified using Test 1-3 from Darvill WWTP (Ekama and Marais, 2002). The dimensions of the SST are shown in Table 3.1. The loading conditions for different tests are shown in Table 3.2, where MLSS represents for influent mixed liquor suspended solids and RAS ratio means RAS flow rate divided by Influent flow rate. The simulated results are also compared with results from "Evaluation of three turbulence models in predicting the steady state hydrodynamics of a secondary sedimentation tank" (Gao & Stenstrom, 2018). The comparison is shown in Figure 3.2.

Table 3.1 Dimension of Darvill SST

Geometry	Value	Unit
Diameter of the clarifier	35	m
Radius of the inlet pipe	0.5	m
Depth of side wall	4.1	m
Stilling well diameter	6	m
Stilling well depth	2.7	m
Stamford baffle depth	0.6	m
Stamford baffle length	1.7	m
Surface area	962	m^2
Tank floor slope	10%	

Table 3.2 Loading conditions for different tests

Test ID	MLSS	RAS ratio	Inlet Q	V_0	r_h	r_p	ρ_p
Unit	g/L		m3/d	m/h	L/g	L/g	kg/m3
Test 1	4.6	0.8	35986	7.71	0.39	10	1450
Test 2	4.3	0.97	32529	7.71	0.39	10	1450
Test 3	3.6	0.79	40726	7.71	0.39	10	1450

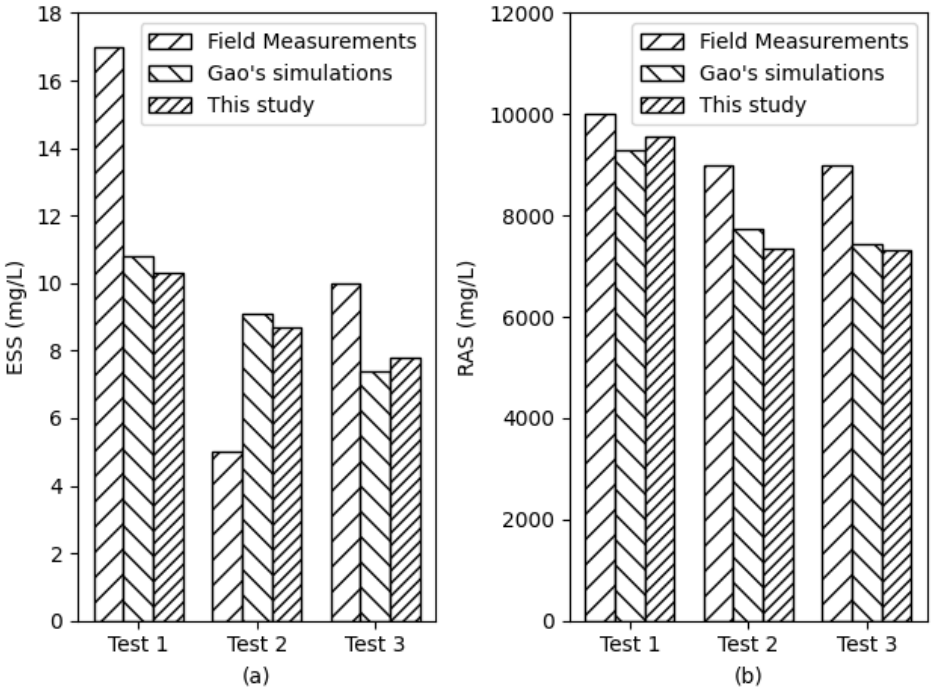

Figure 3.2 Comparison among simulated indicators and previous studies [(a)]ESS, [(b)]RAS

3.4 Simulations Setup

All simulations are steady state and axisymmetric with total iteration steps equal to 50,000. Simulated fluid density, viscosity, and diffusivity are linked to UDF. Three source terms are added to the fluid zone: axial momentum, turbulent kinetic energy, and turbulent dissipation rate.

The inlet boundary condition is a fixed velocity magnitude with a fixed suspend solid concentration value. The outlet boundary condition is set to zero pressure with zero suspend solid concentration flux. The turbulent intensity and hydraulic diameter determine both inlet and outlet turbulent characteristics.

The solution method is the SIMPLE algorithm (Semi-Implicit Method for Pressure Linked Equations). Spatial discretization for the gradient is set to least square cell based. Spatial

discretization for pressure is set to “PRESTO!”. Spatial discretization for all left terms is set to second order upwind. All-over relaxation factors are set to 0.3. Total sludge volume, RAS, and ESS are reported for each time step and are printed in the output file. The data are analyzed later in a Python program. Multiple simulations can be achieved by changing the boundary conditions in the Fluent journal file.

3.5 Scenarios Setup

In this study, a total of three sets of simulations were carried out. In sets A and B, the simulations focus on different combinations of Inlet Q, MLSS (Mixed liquor suspended solids), RAS ratio (ratio of the return activated sludge flux to the inlet flux), and Depth ratio (the ratio of skirt baffle depth to total depth). The combination is determined by Box-Behnken Design which can significantly decrease the simulations needed. All factors have three different values. Twenty-five simulations are designed in each set (compared to eighty-one simulations without Box-Behnken Design).

The range of factors in set A is as follows. Inlet Q (20000-100000 m3/d), MLSS (1000-5000 mg/l), RAS ratio (0.6-1.0), and Depth ratio (0.3-0.9) respectively. The simulation set B is improved from the result of set A. The range of factors in set B is as follows. Inlet Q (10000-40000 m3/d), MLSS (1500-4500 mg/l), RAS ratio (0.75-1.0), and depth ratio (0.3-0.9) respectively. Simulation set B also sets non-settleable solid concentration to 5mg/L compared to 10mg/L in set A. The specific setup is shown in Table 3.3. Simulations in set A have different iteration steps because it was designed to find a better iteration number for later simulations.

In set C, the simulations focus on the influence of baffle depth ratio (from 0.1 to 0.9, with 0.1 as the interval for simulations) and SOR (from 694 to 868, by increasing inlet Q). The

simulations with SOR=694 lb/ft^2-day is contained in C1. The simulations with SOR=781 lb/ft^2-day is contained in C2. And the simulations with SOR=868 lb/ft^2-day is contained in C3. The specific setup is shown in Table 3.4.

Table 3.3 Tests setup A and B

Test ID	Inlet Q	MLSS	RAS ratio	Depth ratio	Effluent Q	Test ID	Inlet Q	MLSS	RAS ratio	Depth ratio	Effluent Q
Unit	m3/d	mg/l			m3/d	Unit	m3/d	mg/l			m3/d
A1	20000	3000	0.80	0.3	11111	B1	10000	3000	1.00	0.3	5000
A2	60000	1000	0.80	0.3	33333	B2	25000	1500	1.00	0.3	12500
A3	60000	3000	0.60	0.3	37500	B3	25000	3000	0.75	0.3	14286
A4	60000	3000	1.00	0.3	30000	B4	25000	3000	1.25	0.3	11111
A5	60000	5000	0.80	0.3	33333	B5	25000	4500	1.00	0.3	12500
A6	100000	3000	0.80	0.3	55556	B6	40000	3000	1.00	0.3	20000
A7	20000	1000	0.80	0.6	11111	B7	10000	1500	1.00	0.6	5000
A8	20000	3000	0.60	0.6	12500	B8	10000	3000	0.75	0.6	5714
A9	20000	3000	1.00	0.6	10000	B9	10000	3000	1.25	0.6	4444
A10	20000	5000	0.80	0.6	11111	B10	10000	4500	1.00	0.6	5000
A11	60000	1000	0.60	0.6	37500	B11	25000	1500	0.75	0.6	14286
A12	60000	1000	1.00	0.6	30000	B12	25000	1500	1.25	0.6	11111
A13	60000	3000	0.80	0.6	33333	B13	25000	3000	1.00	0.6	12500
A14	60000	5000	0.60	0.6	37500	B14	25000	4500	0.75	0.6	14286
A15	60000	5000	1.00	0.6	30000	B15	25000	4500	1.25	0.6	11111
A16	100000	1000	0.80	0.6	55556	B16	40000	1500	1.00	0.6	20000
A17	100000	3000	0.60	0.6	62500	B17	40000	3000	0.75	0.6	22857
A18	100000	3000	1.00	0.6	50000	B18	40000	3000	1.25	0.6	17778
A19	100000	5000	0.80	0.6	55556	B19	40000	4500	1.00	0.6	20000
A20	20000	3000	0.80	0.9	11111	B20	10000	3000	1.00	0.9	5000
A21	60000	1000	0.80	0.9	33333	B21	25000	1500	1.00	0.9	12500
A22	60000	3000	0.60	0.9	37500	B22	25000	3000	0.75	0.9	14286
A23	60000	3000	1.00	0.9	30000	B23	25000	3000	1.25	0.9	11111
A24	60000	5000	0.80	0.9	33333	B24	25000	4500	1.00	0.9	12500
A25	100000	3000	0.80	0.9	55556	B25	40000	3000	1.00	0.9	20000

Table 3.4 Tests setup C

Test ID	Inlet Q	MLSS	RAS ratio	Depth ratio	SOR
Unit	m3/d	mg/l			lb/ft2-day
C1-1	40000	3000	1.00	0.1	694
C1-2	40000	3000	1.00	0.2	694
C1-3	40000	3000	1.00	0.3	694
C1-4	40000	3000	1.00	0.4	694
C1-5	40000	3000	1.00	0.5	694
C1-6	40000	3000	1.00	0.6	694
C1-7	40000	3000	1.00	0.7	694
C1-8	40000	3000	1.00	0.8	694
C1-9	40000	3000	1.00	0.9	694
C2-1	45000	3000	1.00	0.1	781
C2-2	45000	3000	1.00	0.2	781
C2-3	45000	3000	1.00	0.3	781
C2-4	45000	3000	1.00	0.4	781
C2-5	45000	3000	1.00	0.5	781
C2-6	45000	3000	1.00	0.6	781
C2-7	45000	3000	1.00	0.7	781
C2-8	45000	3000	1.00	0.8	781
C2-9	45000	3000	1.00	0.9	781
C3-1	50000	3000	1.00	0.1	868
C3-2	50000	3000	1.00	0.2	868
C3-3	50000	3000	1.00	0.3	868
C3-4	50000	3000	1.00	0.4	868
C3-5	50000	3000	1.00	0.5	868
C3-6	50000	3000	1.00	0.6	868
C3-7	50000	3000	1.00	0.7	868
C3-8	50000	3000	1.00	0.8	868
C3-9	50000	3000	1.00	0.9	868

4 Results and Discussion

4.1 Set A and Set B

The average ESS and RAS values of test sets A and B are shown in Table 4.1. The average is taken from the last 10,000 steps when the simulations became more stable than earlier simulations. Detailed analysis will be done later.

The Pearson correlation coefficients for Set A and Set B are shown in Table 4.2. The ESS is highly related to the Inlet Q (0.823 and 0.635) for both Set A and Set B. The RAS is highly related to the MLSS (0.829 and 0.946) for both Set A and Set B. The RAS ratio and Depth ratio are minor factors. They have a more significant impact on RAS (around ten times the Pearson correlation coefficients than ESS).

Table 4.1 Average ESS and RAS values of test sets A and B

Test ID	ESS	RAS	Test ID	ESS	RAS
	mg/l	mg/l		mg/l	mg/l
A1	10.03	5986	B1	5.03	5657
A2	14.47	2176	B2	6.94	2801
A3	15.24	7348	B3	6.02	6677
A4	12.79	5840	B4	5.65	5158
A5	15.86	8381	B5	6.00	7972
A6	28.08	5030	B6	7.20	5853
A7	11.26	1957	B7	5.14	2628
A8	10.74	7504	B8	5.09	6576
A9	10.23	5718	B9	5.05	5084
A10	10.11	9607	B10	5.04	7718
A11	18.63	2518	B11	8.20	3284
A12	15.40	1886	B12	6.81	2517
A13	17.02	6623	B13	5.73	5754
A14	19.49	9276	B14	6.22	9046
A15	29.36	8476	B15	10.69	7099
A16	21.34	2152	B16	9.66	2855
A17	22.63	5583	B17	7.45	6575
A18	28.09	5145	B18	7.16	5255
A19	26.70	6387	B19	7.01	7767

A20	10.12	6393	B20	5.01	6180
A21	14.44	1238	B21	5.73	2729
A22	15.24	2952	B22	6.29	6185
A23	13.32	3119	B23	5.44	5194
A24	23.91	4928	B24	6.86	7109
A25	23.53	3145	B25	7.41	5290

Table 4.2 Pearson correlation coefficients for Set A (1st) and Set B (2nd)

	[1]A	[2]B	[3]C	[4]D	AB	AC	AD
ESS-1st	0.823	0.280	0.068	0.038	0.780	0.800	0.647
RAS-1st	-0.229	0.829	-0.118	-0.306	0.372	-0.247	-0.379
ESS-2nd	0.635	-0.027	0.063	-0.003	0.420	0.602	0.477
RAS-2nd	-0.008	0.946	-0.254	-0.045	0.584	-0.103	-0.047
	BC	BD	CD	A^2	B^2	C^2	D^2
ESS-1st	0.312	0.270	0.065	0.808	0.305	0.068	0.007
RAS-1st	0.727	0.444	-0.315	-0.204	0.782	-0.108	-0.334
ESS-2nd	0.057	0.008	0.020	0.597	0.035	0.072	-0.049
RAS-2nd	0.718	0.616	-0.149	-0.001	0.907	-0.246	-0.044

[1]A represents for Inlet Q; [2]B represents for MLSS; [3]C represents for RAS ratio; [4]D represents for Depth ratio.

4.1.1 ESS of Set A

In this study, the value of ESS is reported every ten iterations. Some pilot simulations are carried out. The results show that there is a huge variation in the ESS value due to the turbulence effect. Here, the ESS plots in Set A are divided into three types. Type I: steady or slightly fluctuating (as shown in Figure 4.1). Type II: unstable or highly fluctuating (as shown in Figure 4.2). Type III: failure (as shown in Figure 4.3). It is worth noticing that simulations with higher SOR or SLR tend to have ESS plots appear unstable or failed. In Set B, the SOR is in the range which will not cause failure. The variance of ESS in the last 10,000 iterations will be investigated later.

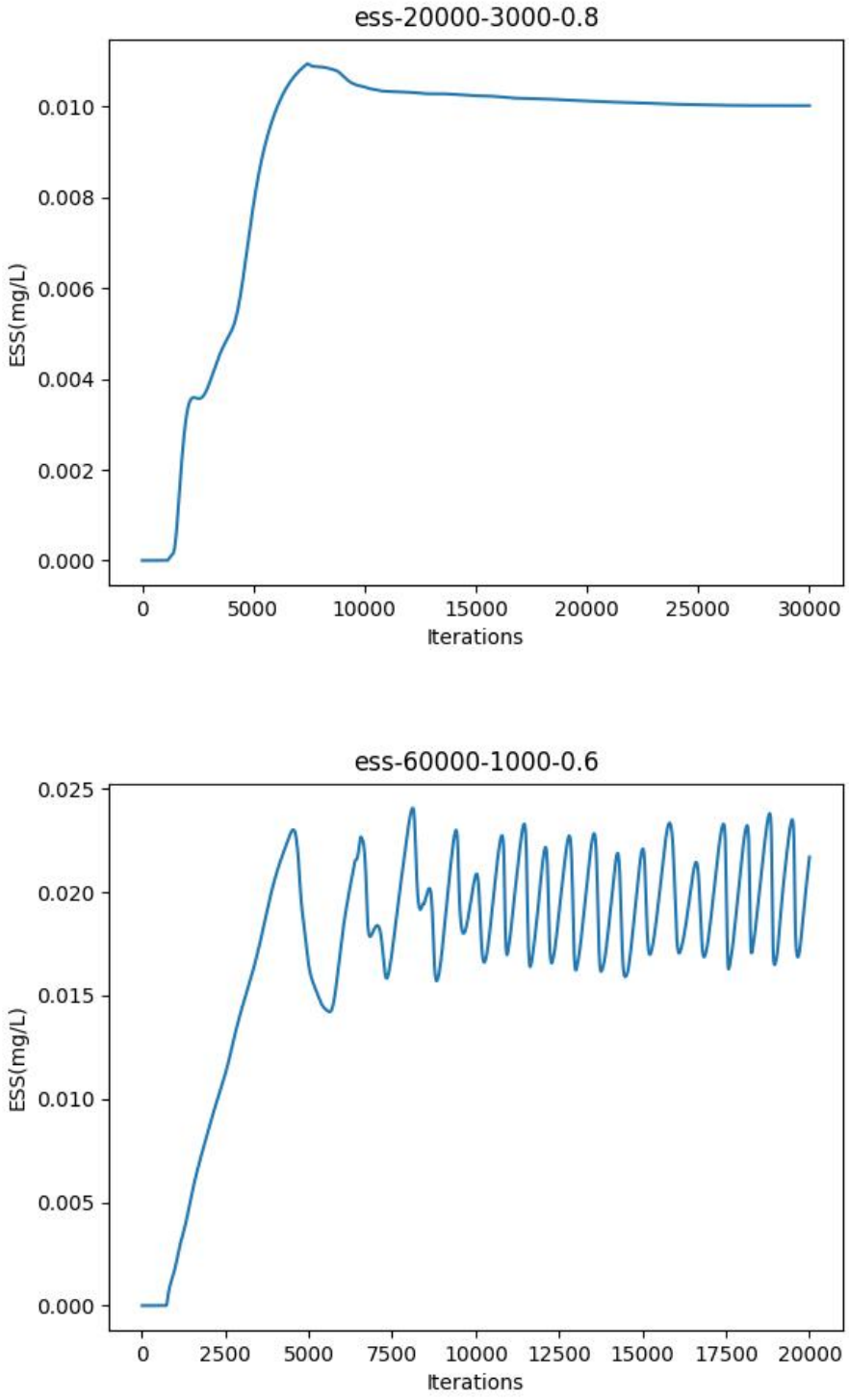

Figure 4.1 Type I: steady or slightly fluctuating

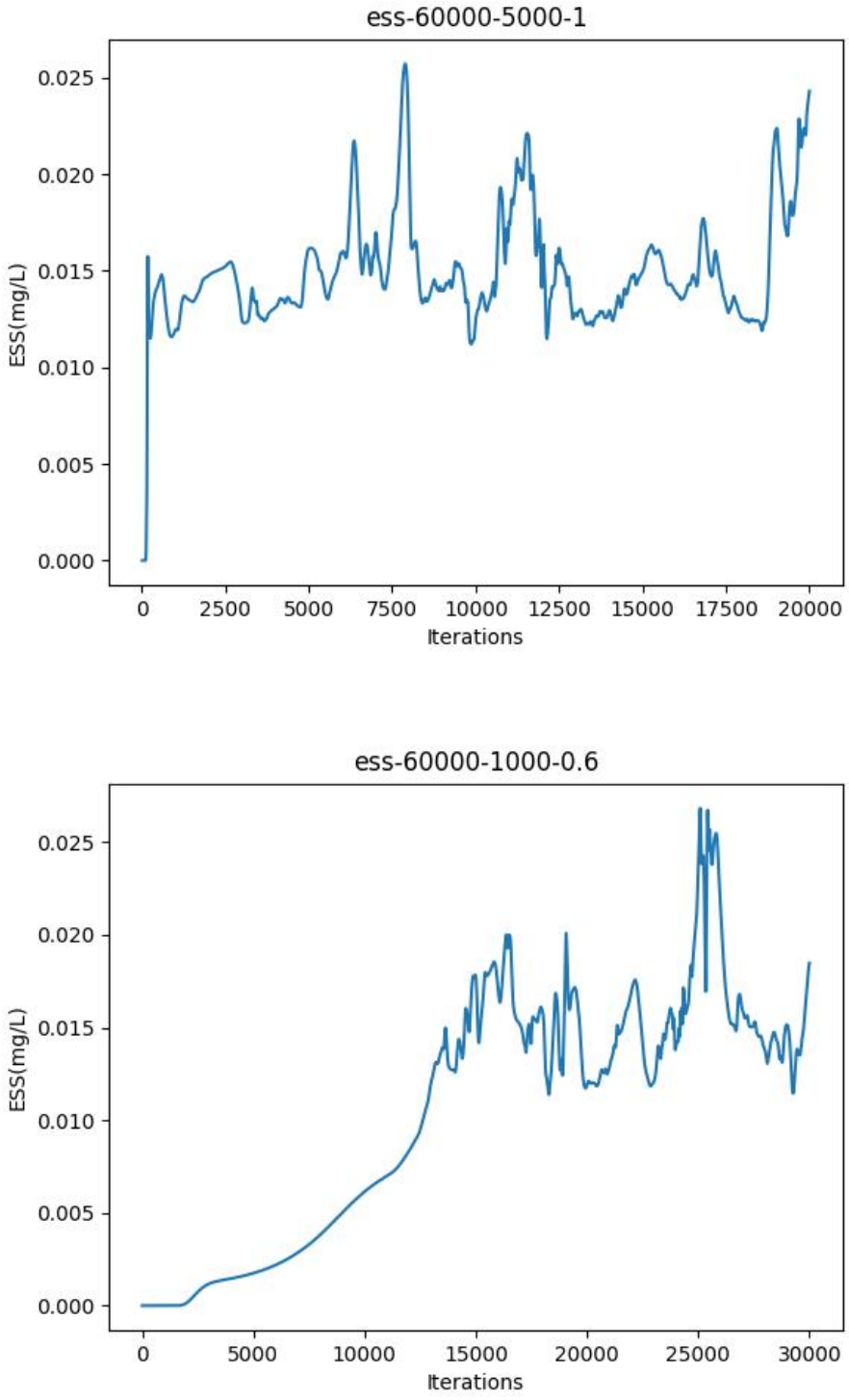

Figure 4.2 Type II: highly fluctuating

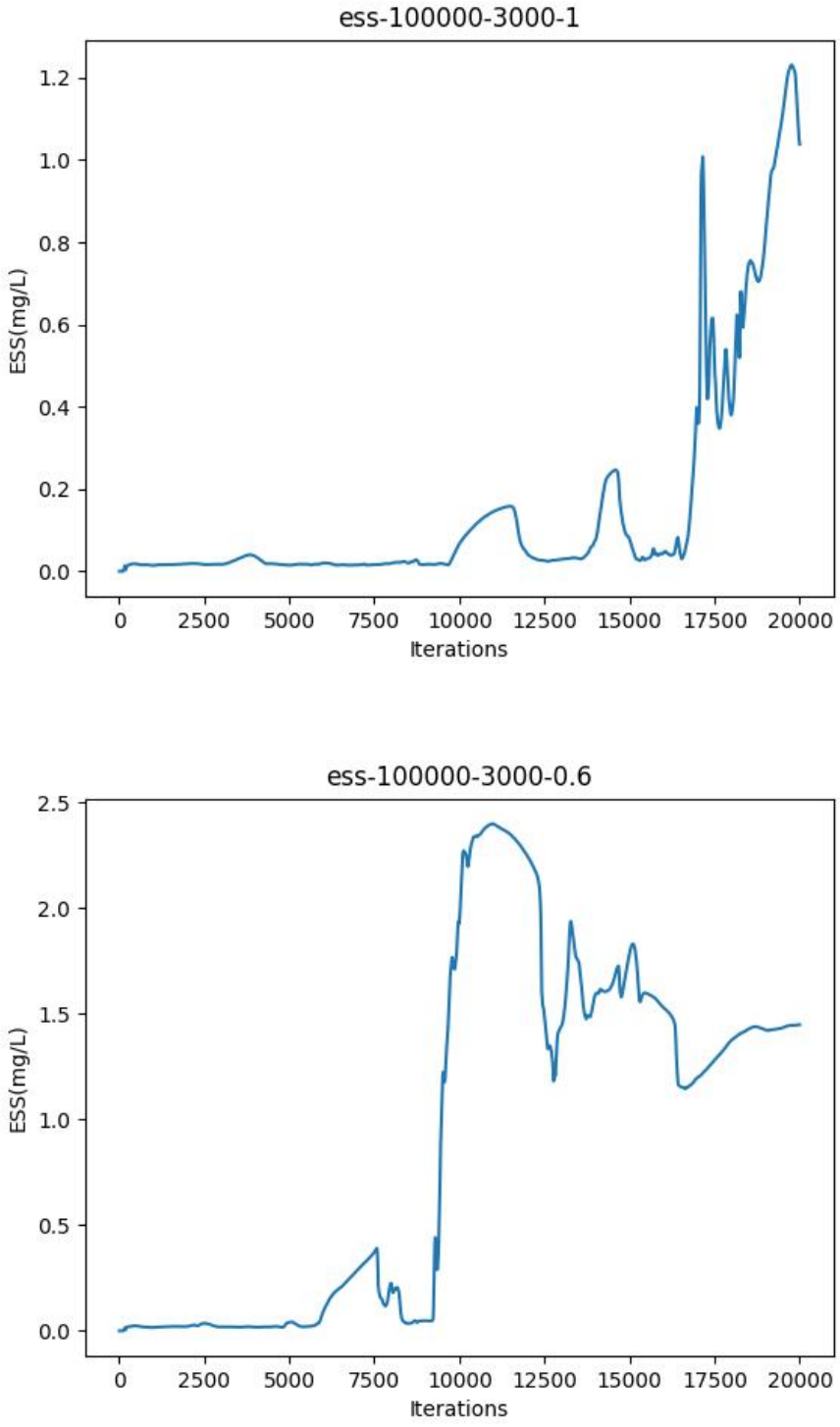

Figure 4.3 Type III: failure

4.1.2 ESS of Set B

Here, the plot of standard deviation of ESS values in Set B is shown in Figure 4.4. It can be found clearly that higher SOR tends to have a higher variance. The trend means that those unstable SST operating conditions also tends to have a higher numerical diffusion in the simulation. It also implies that if an unstable simulation is obtained, that operation is much likely to fail.

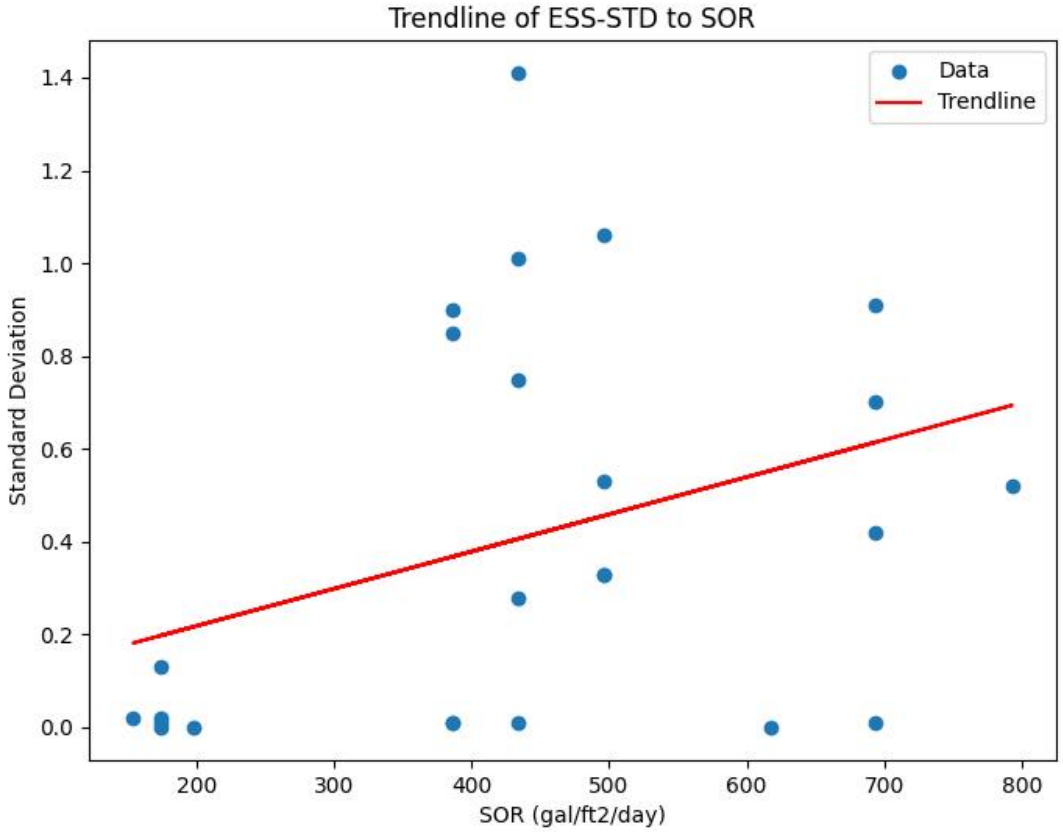

Figure 4.4 Standard deviation of ESS in Set B

4.1.3 RAS

The RAS results are much more stable than ESS. A representative RAS plot is shown in Figure 4.5. The simulated RAS values are compared to the predicted RAS in Table 4.3. Predicted RAS is the RAS calculated from the conservation equation when the SST reaches a steady state. The equation can be found in equation (11). It is worth noticing that predicted RAS is always higher than simulated RAS. It might be caused by insufficient iterations which prevent the simulation reaching a steady state.

$$pRAS = \frac{Q_{in} * MLSS - (Q_{in} - Q_R) * ESS}{Q_R} \tag{10}$$

where $pRAS$ is predicted RAS; Q_{in} is influent flux; and Q_R is the returning flux.

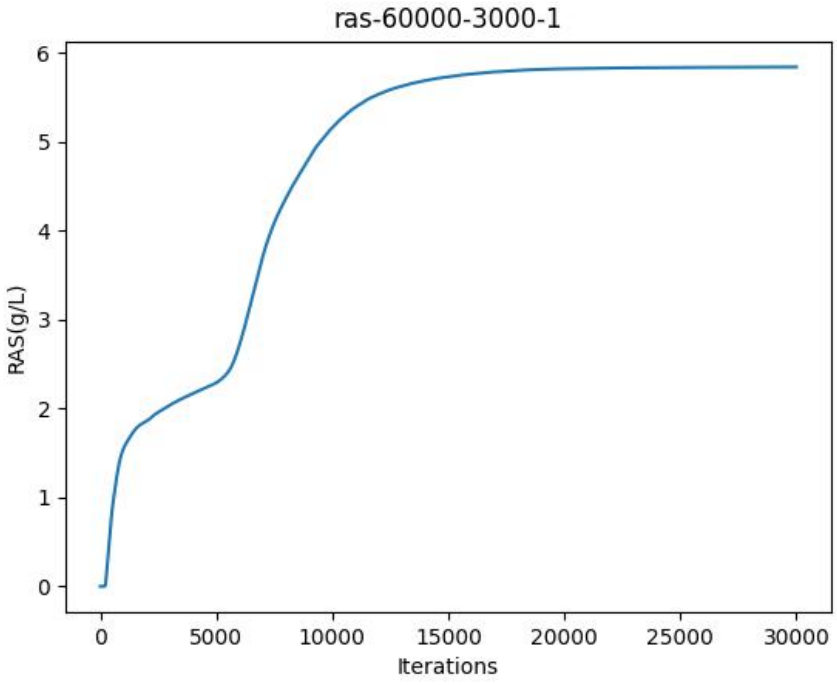

Figure 4.5 Representative RAS-iterations plot

Table 4.3 RAS values for simulation Set B

Test ID	Simulated RAS	Predicted RAS	Difference
Unit	mg/l	mg/l	mg/l
B1	5656	5995	339
B2	2802	2993	191
B3	6676	6992	316
B4	5157	5395	239
B5	7926	8994	1068
B6	5854	5993	139
B7	2631	2995	364
B8	6572	6993	421
B9	5083	5396	313
B10	7705	8995	1290
B11	3281	3489	208
B12	2516	2695	179
B13	5752	5994	242
B14	8951	10492	1541
B15	7098	8091	994
B16	2854	2990	136
B17	6593	6990	397
B18	5255	5394	139
B19	7737	8993	1256
B20	6181	5995	-186
B21	2729	2994	265
B22	6176	6992	816
B23	5187	5396	209
B24	7115	8993	1878
B25	5260	5993	733

4.1.4 Short conclusions for Set A and B

In simulations set A and set B, the relation between ESS and stability is investigated. Unstable SST operating conditions also tend to have a higher numerical diffusion in the simulation. The RAS results are more stable. Simulation set C is designed based on these findings.

4.2 Set C

Simulation set C is designed to determine the optimal baffle depth for the particular SST. The method can be intriguing for other SST designs and optimization based on CFD simulations. The plots of ESS values for different depth ratios (baffle depth to total depth) are shown in Figures 4.6, 4.7, 4.8, with SOR equals 694 gal/ft2/day, 781 gal/ft2/day and 868 gal/ft2/day, respectively. Only representative depth ratios are plotted. Full plots can be found in the appendix. When the depth ratio equals 0.1, 0.2, and 0.9, the ESS values tend to be unstable for these SOR values. As mentioned in section 4.1, higher variance means there is a higher probability of failure. This phenomenon implies that too shallow or too deep baffle tends to have worse performance for this SST under the same operation scenario.

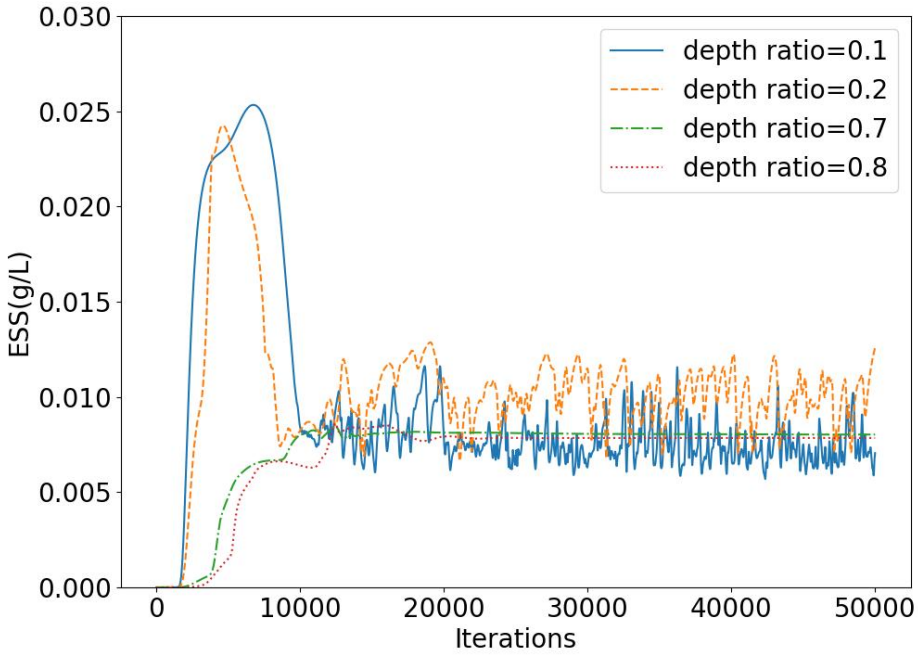

Figure 4.6 ESS values of different depth ratios SOR=694 gal/ft2/day

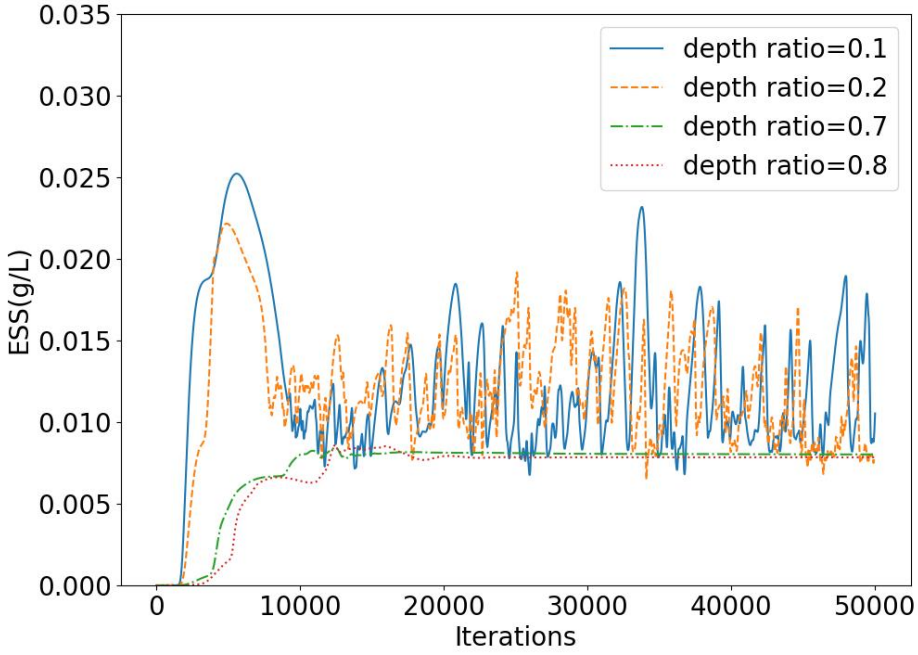

Figure 4.7 ESS values of different depth ratios SOR=781 gal/ft2/day

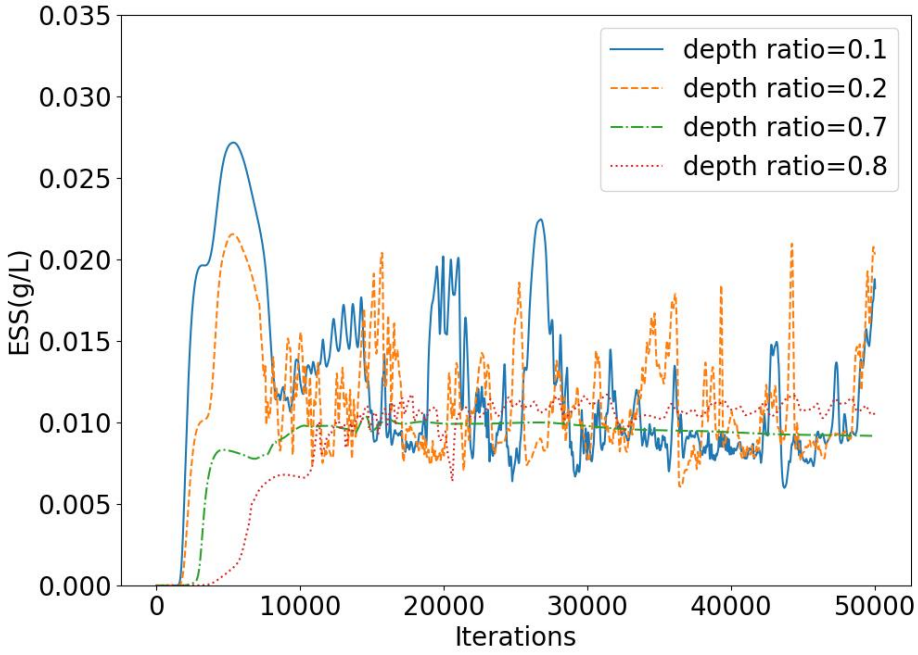

Figure 4.8 ESS values of different depth ratios SOR=868 gal/ft2/day

The sludge concentration contours of different depth ratios for three different SOR values are shown in Figure 4.9. When depth ratio equals 0.1, there seems to be some abnormal patterns for the depth of sludge blanket. For depth ratio equal to 0.3, 0.5, 0.7, the intersections of sludge blanket appear as a wave line. When depth ratio equals to 0.7 and SOR equals to 694 gal/ft^2/day, the intersection appears like a straight line. And the amplitude of the wave lines at depth ratio 0.7 is significantly lower than other depth ratio regardless of SOR values. When depth ratio equals to 0.9, the SST failed when the SOR equals to 781 gal/ft^2/day and 868 gal/ft^2/day. The failure can be explained by blocking effect of the baffle on returning flow. The sludge blanket depth is also significantly higher than other depth ratio. The detailed numerical analysis can be found later.

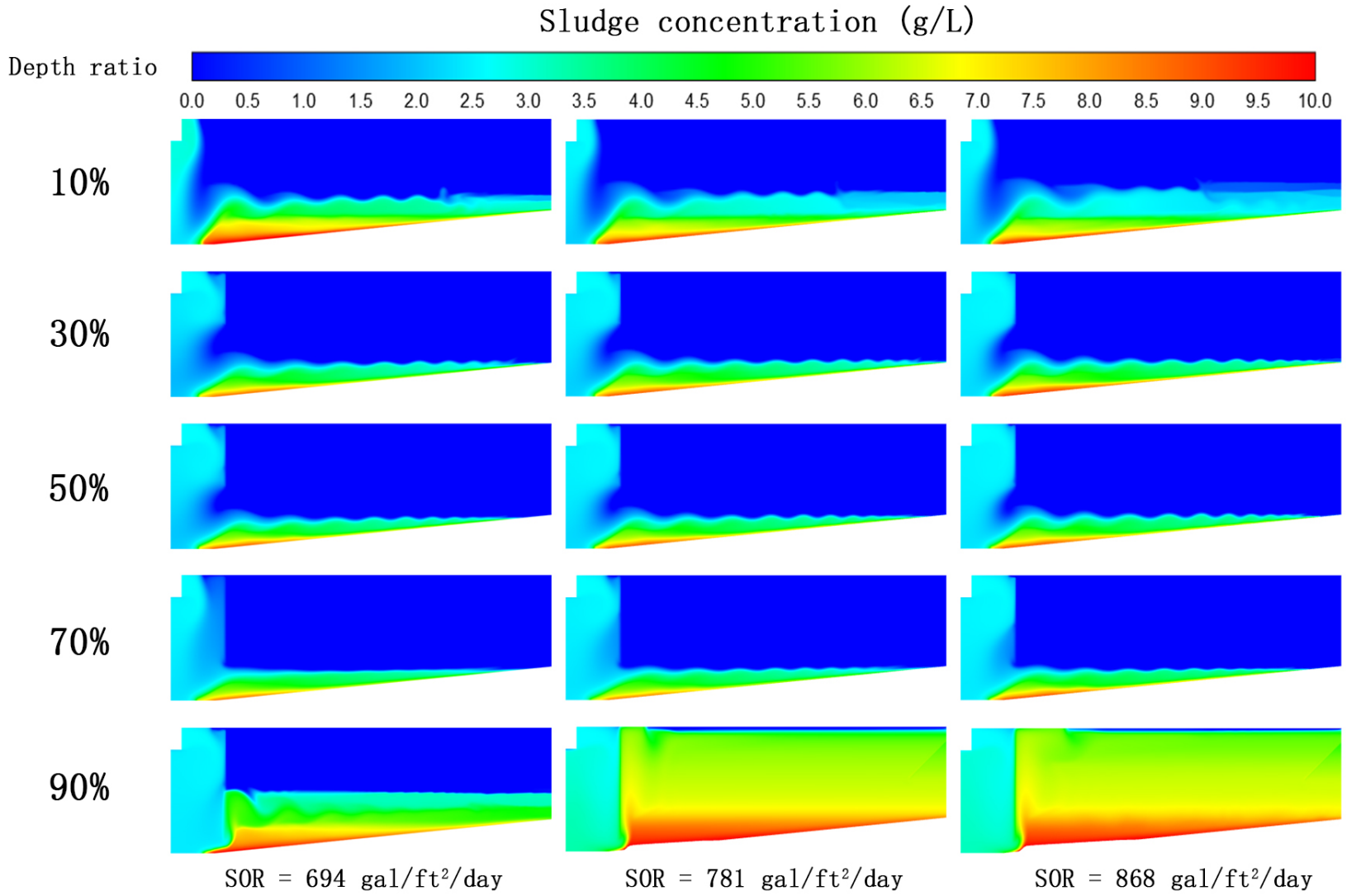

Figure 4.9 Sludge concentration contours of different depth ratios

The ESS values, sludge mass, and sludge blanket height plots are shown in Figure 4.10, 4.11, 4.12, respectively. The plots utilize data with interpolation from ten different depths. Figure 4.10 is log scale because the ESS values at 0.9 depth ratio is much higher than that at other depth ratio when SOR is large. Those figures show a similar trend with the features tending to decrease when the baffle extends to a depth approaching a depth ratio 0.9. The optimal depth ratio can be assumed to be around 0.7 for this SST.

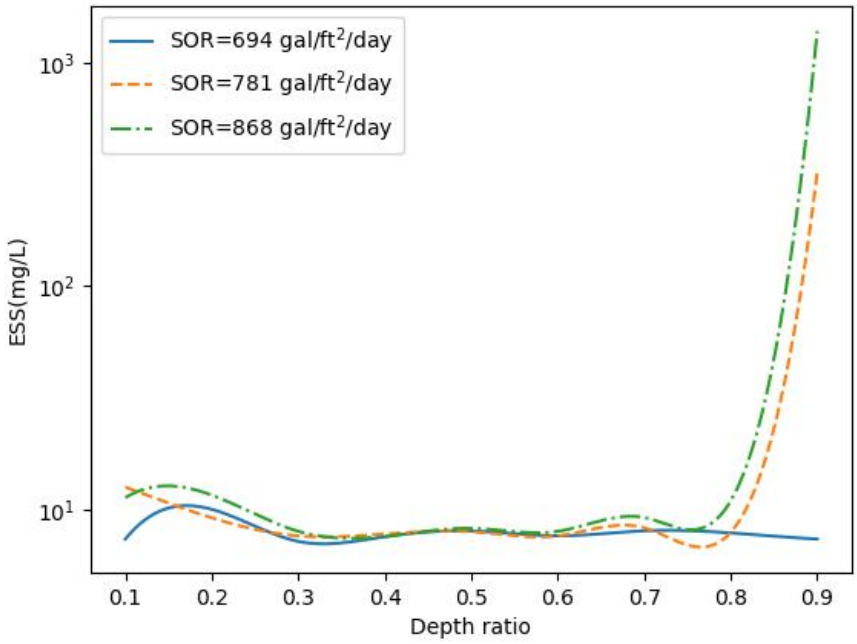

Figure 4.10 The relationship between ESS and depth ratio

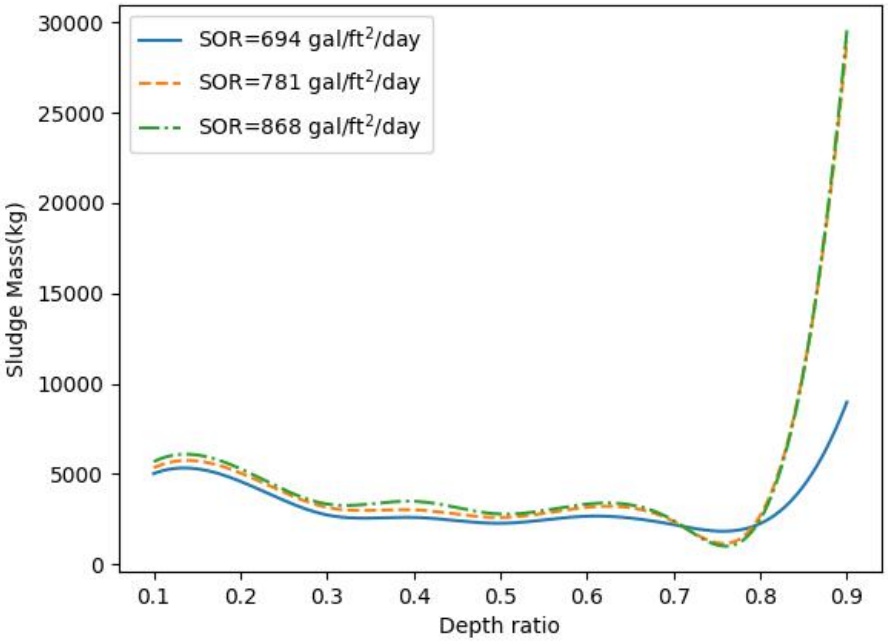

Figure 4.11 The relationship between total sludge mass and depth ratio

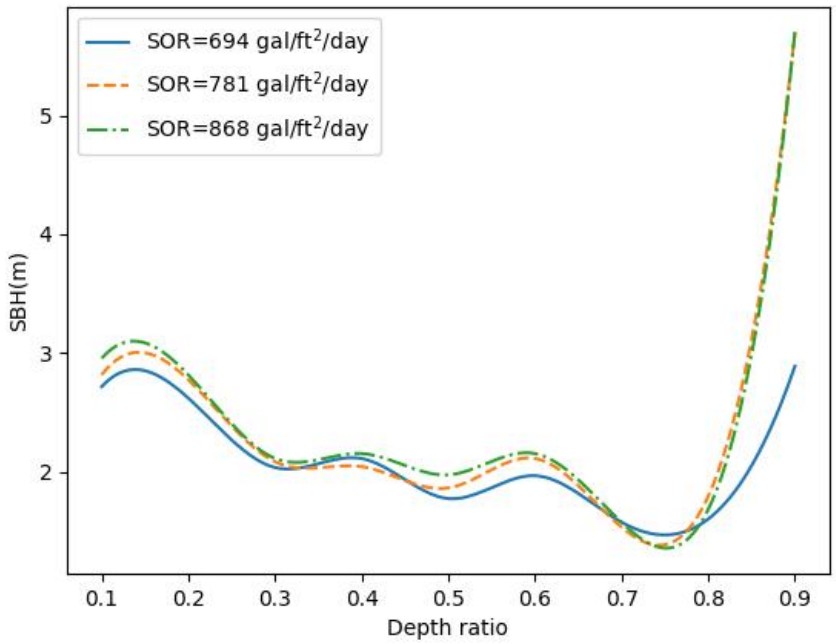

Figure 4.12 The relationship between SBH and depth ratio

5 Conclusions

In this study, a series of simulations were conducted using Fluent® to determine the ideal skirt well depth. Some conclusions can be made as follows.1. The numerical stability of simulated ESS concentration depends on SOR. Simulations are divided into three types. Type I stands for stable results. Type II stands for oscillating results. Type III stands for failure results. It was discovered that simulations with larger SOR tend to produce more Type III outcomes, implying that the SST is more likely to fail. In simulation set B, the trend line of standard deviation to SOR is plotted. The positive slope of the trend line implies that a higher SOR will result in a higher standard deviation in ESS concentration.

2. The concentration of the simulated RAS is much more stable. The simulated RAS concentration is often lower than the RAS concentration calculated from the conservative equation. This may be due to a lack of iterations in the simulation.

3. Desired skirt well depth is around 0.7 of the total depth. When the baffle is too shallow, the ESS concentration is very unstable and more likely to fail under higher SOR. When the baffle is excessively deep, the returned sludge is blocked, resulting in higher SBH and decreased SST capacity.

This MS thesis provides a feasible way to design or reform skirt baffle depth by multiple CFD simulations.

6 References

Ardern, E., & Lockett, W. T. (1914). Experiments on the oxidation of sewage without the aid of filters. Journal of the society of chemical industry, 33(10), 523-539.

Batchelor, G. K. (1973). An Introduction to Fluid Dynamics. Cambridge University Press.

Bokil, S. D. (1972). Effect of Mechanical Blending on the Aerobic Digestion of the Waste Activated Sludge [Doctoral dissertation,University of Windsor]. Ontario, Canada.

Brennen, C. E., & Brennen, C. E. (2005). Fundamentals of multiphase flow. Cambridge University Press.

Bryant, J. O. (1972). Continuous Time Simulation of the Conventional Activated Sludge Wastewater Renovation System [Doctoral dissertation, Clemson University]. South Carolina, US.

Burt, D. J. (2010). Improved design of settling tanks using an extended drift flux model [Doctoral dissertation, University of Bristol]. Bristol, UK.

Dahl, C., Larsen, T., & Petersen, O. (1994). Numerical modelling and measurement in a test secondary settling tank. Water Science and Technology, 30(2), 219.

De Clercq, B. (2004). Computational fluid dynamics of settling tanks: Development of experiments and rheological, settling, and scraper submodels [Doctoral dissertation, Ghent University]. Ghent, Belgium.

Dobbins, W. E. (1944). Effect of turbulence on sedimentation. Transactions of the American Society of Civil Engineers, 109(1), 629-656.

Ekama, G. A., Barnard, J. L., Gunthert, F. W., Krebs, P., McCorquodale, J. A., Parker, D. S., & Wahlberg, E. J. (1997). Secondary Settling Tanks: Theory, Modelling, Design and Operation. IWA Publishing.

Gao, H. W. (2016). Verification modeling study for the influential factors of secondary clarifier [Master's thesis, University of California Los Angeles]. Los Angeles, US.

Gao, H. W., & Stenstrom, M. K. (2018). Evaluation of three turbulence models in predicting the steady state hydrodynamics of a secondary sedimentation tank. Water Research, 143, 445-456.

Gao, H. W., & Stenstrom, M. K. (2020a, May 17-21). Computational Fluid Dynamics Analysis for Improving Secondary Settling Tank Performance. [Proceedings Paper]. 20th Annual World Environmental and Water Resources Congress, Henderson, NV.

Gao, H. W., & Stenstrom, M. K. (2020b). The influence of wind in secondary settling tanks for wastewater treatment - A computational fluid dynamics study. Part II: Rectangular secondary settling tanks. Water Environment Research, 92(4), 551-561.

Gerges, H., & McCorquodale, A. (2008). Thirty years of sedimentation tanks modeling learning from experience. In WEFTEC 2008 (pp. 1613-1619). Water Environment Federation.

Haug, R. T., Cheng, P. P., Hartnett, W. J., Tekippe, R. J., Rad, H., & Esler, J. (1999). LA's New Clarifier Inlet Nearly Doubles Hydraulic Capacity. Proc. In Water Environ. Fed. 72nd Annu. Conf. Exposition.

Hazen, A. (1904). On sedimentation. Transactions of the American Society of Civil Engineers, 53(2), 45-71.

Kynch, G. J. (1952). A theory of sedimentation. Transactions of the Faraday society, 48, 166-176.

Lainé, S., Phan, L., Pellarin, P., & Robert, P. (1999). Operating diagnostics on a flocculator-settling tank using Fluent CFD software. Water Science and Technology, 39(4), 155-162.

Lakehal, D., Krebs, P., Krijgsman, J., & Rodi, W. (1999). Computing shear flow and sludge blanket in secondary clarifiers. Journal of Hydraulic Engineering, 125(3), 253-262.

Larsen, P. (1977). On the hydraulics of rectangular settling basins: experimental and theoretical studies. Department of Water Resources Engineering, Lund Institute of Technology, University of Lund.

Malcherek, A. (1994). Numerical modelling of cohesive settling velocities. Int. J. of Sediment Research, 9(97), 106.

McCorquodale, J. A., La Motta, E. J., Griborio, A., Homes, J., & Georgiou, I. (2004). Development of software for modeling activated sludge clarifier systems. A Technology Transfer Report, Department of Civil and Environmental Engineering, University of New Orleans, LA, 70148.

Stenstrom, M. K. (1976). A dynamic model and computer compatible control strategies for wastewater treatment plant [Doctoral dissertation, Clemson University]. South Carolina, US.

Takács, I., Patry, G. G., & Nolasco, D. (1991). A dynamic model of the clarification-thickening process. Water Research, 25(10), 1263-1271.

Tekippe, R. J. (2002, January). Secondary settling tank inlet design: full scale test results lead to optimization. In WEFTEC 2002 (pp. 522-551). Water Environment Federation.

Vesilind, P. A. (1968). The influence of stirring in the thickening of biological sludge. The University of North Carolina at Chapel Hill.

Vitasovic, Z. C., Zhou, S., McCorquodale, J. A., & Lingren, K. (1997). Secondary clarifier analysis using data from the Clarifier Research Technical Committee protocol. Water Environment Research, 69(5), 999-1007.

Vitasovic, Z. Z. (1986). AN INTEGRATED CONTROL STRATEGY FOR THE ACTIVATED SLUDGE PROCESS [Doctoral dissertation, Rice University]. Houston, US.

7 Appendix

The naming rule for the following plots is Influent Q (m^3/day) - Influent MLSS (mg/L) - RAS ratio - baffle depth ratio. The plots are arranged in an order of increasing depth for the baffle.

7.1 Set C: ESS at SOR=694 gal/ft2/day

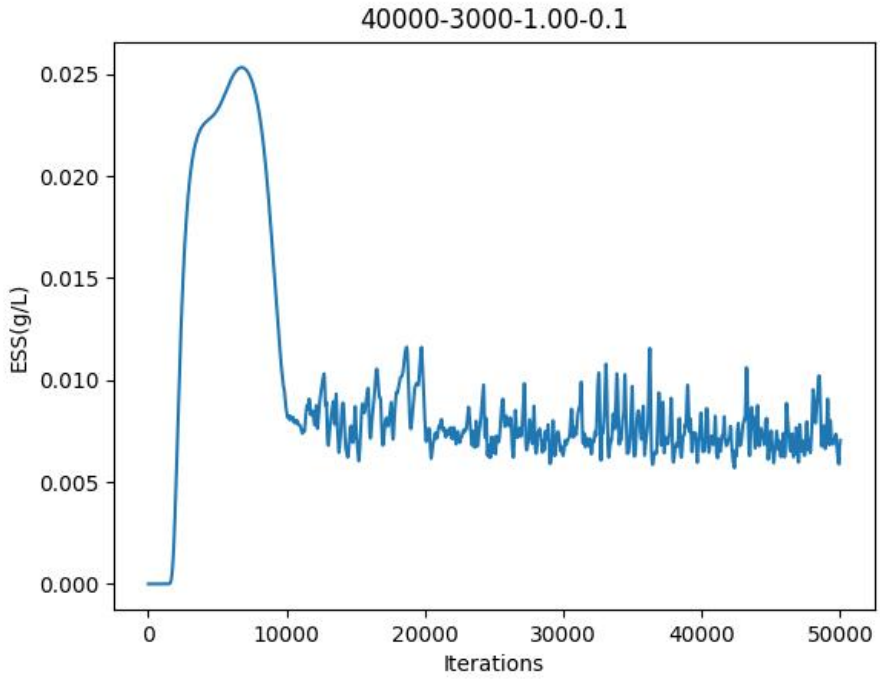

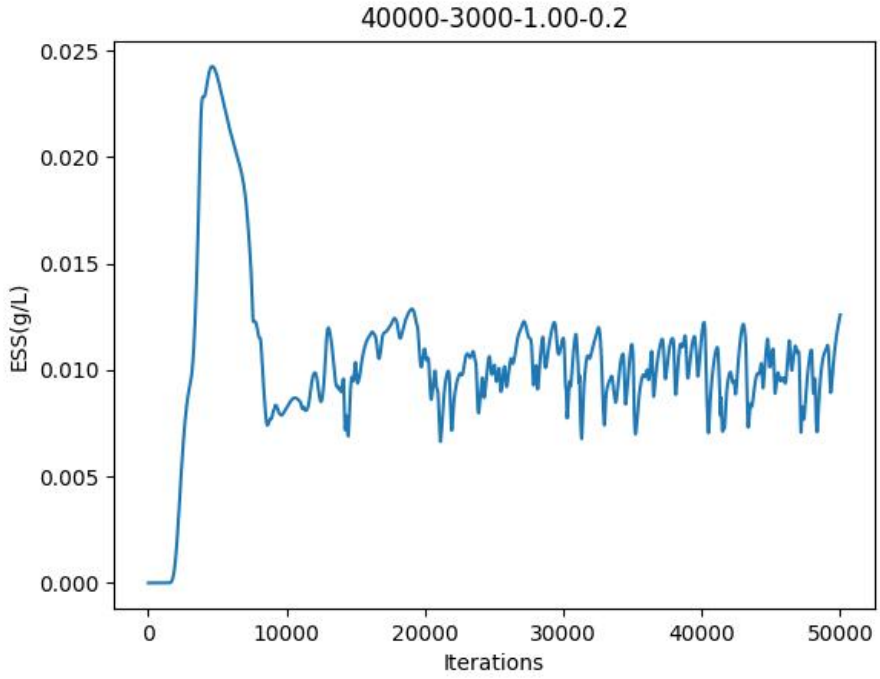
40000-3000-1.00-0.2
0.025
0.020
0.015
0.010
0.005
0.000
ESS(g/L)
0
10000
20000
30000
40000
50000
Iterations

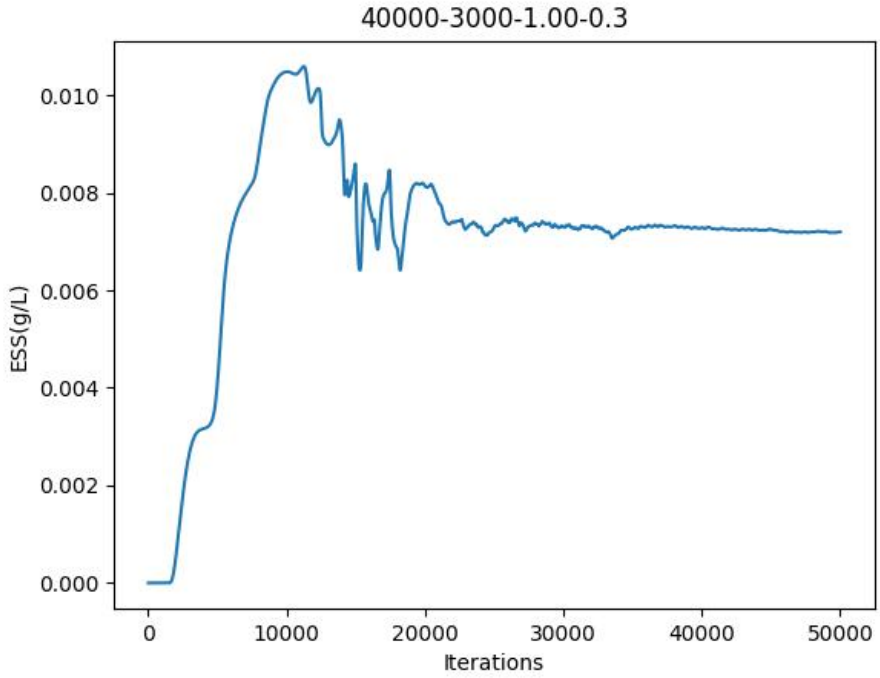
40000-3000-1.00-0.3
0.010
0.008
0.006
0.004
0.002
0.000
ESS(g/L)
0
10000
20000
30000
40000
50000
Iterations

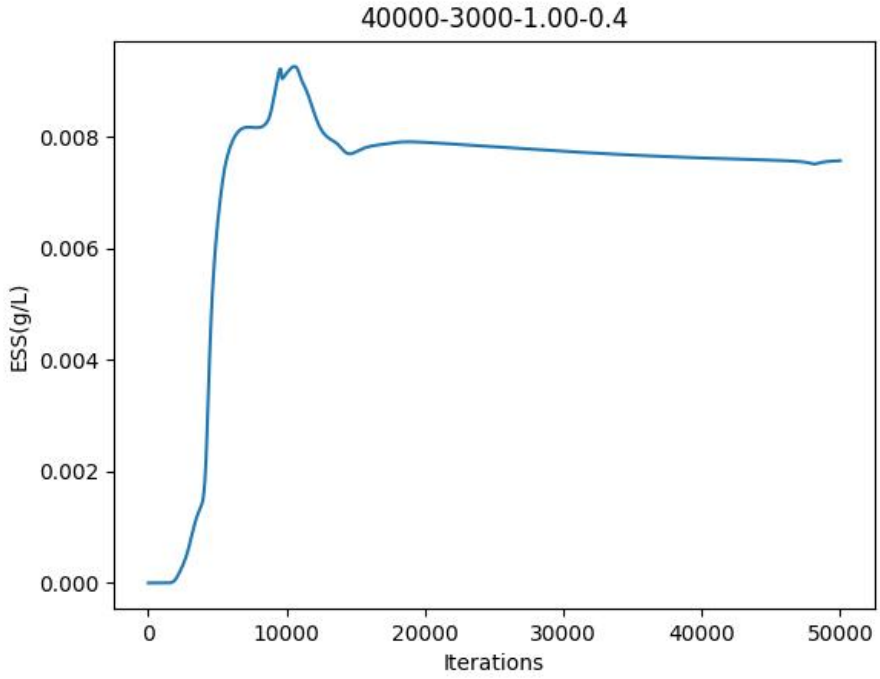
40000-3000-1.00-0.4
ESS(g/L)
0.000
0.002
0.004
0.006
0.008
0
10000
20000
30000
40000
50000
Iterations

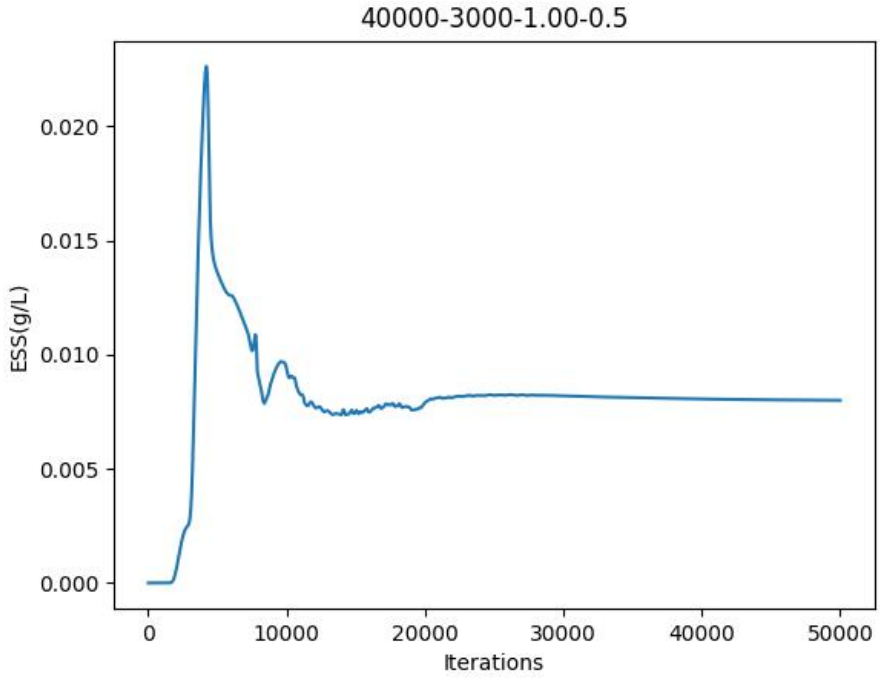
40000-3000-1.00-0.5
ESS(g/L)
0.000
0.005
0.010
0.015
0.020
0
10000
20000
30000
40000
50000
Iterations

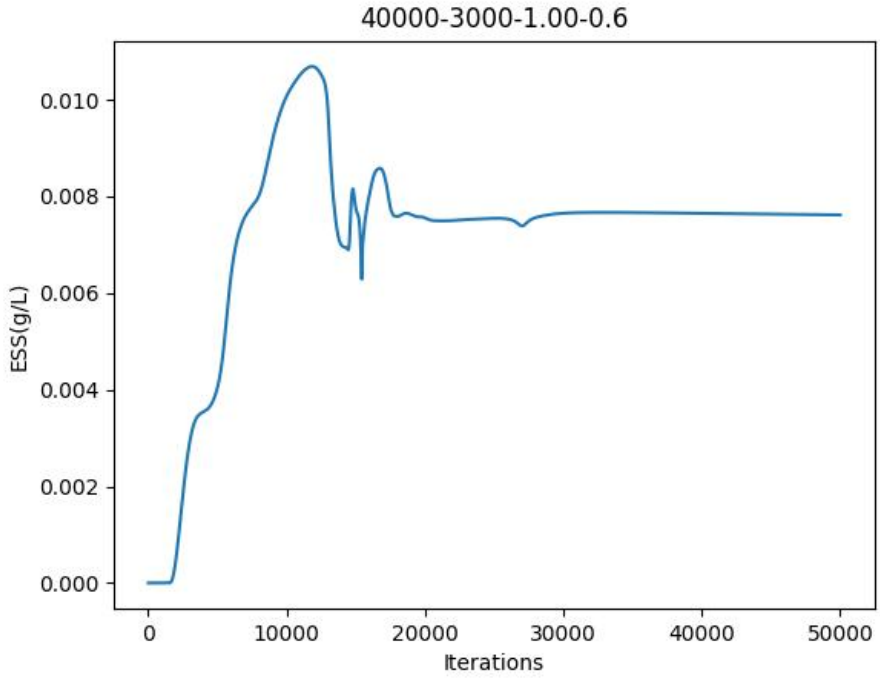
40000-3000-1.00-0.6
0.010
0.008
0.006
0.004
0.002
0.000
ESS(g/L)
0
10000
20000
30000
40000
50000
Iterations

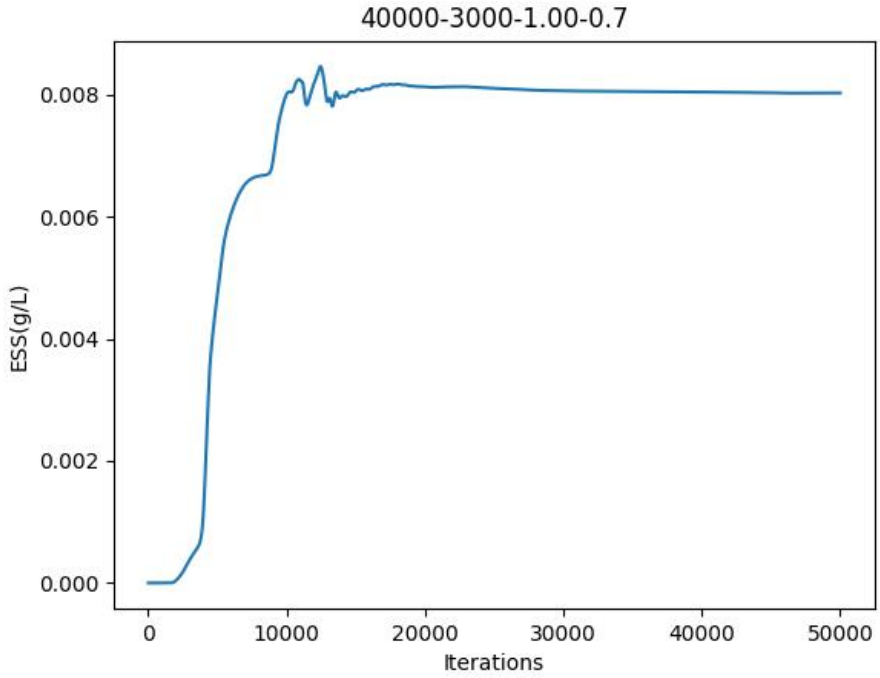
40000-3000-1.00-0.7
0.008
0.006
0.004
0.002
0.000
ESS(g/L)
0
10000
20000
30000
40000
50000
Iterations

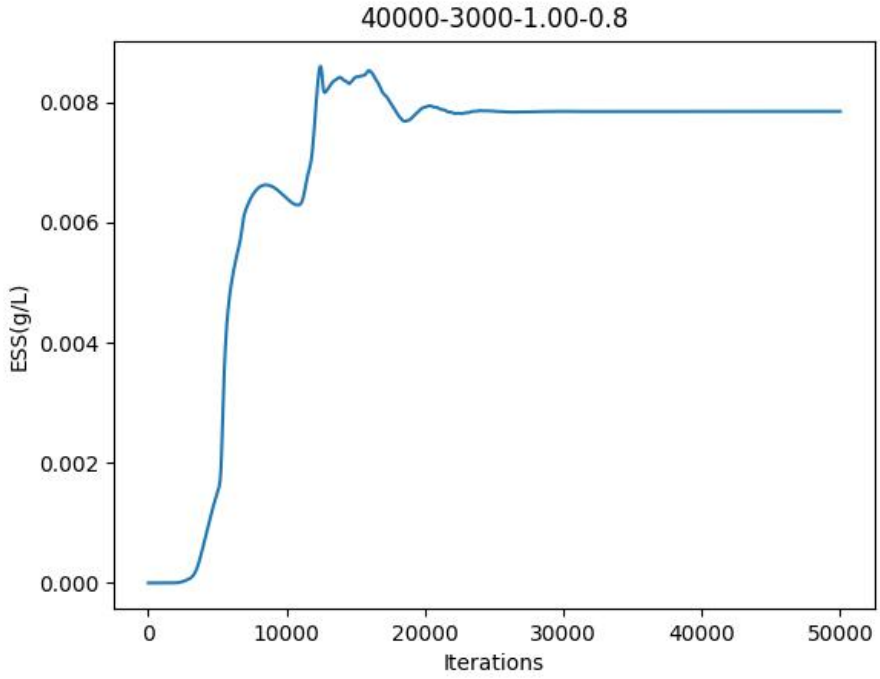
40000-3000-1.00-0.8
ESS(g/L)
0.000
0.002
0.004
0.006
0.008
0
10000
20000
30000
40000
50000
Iterations

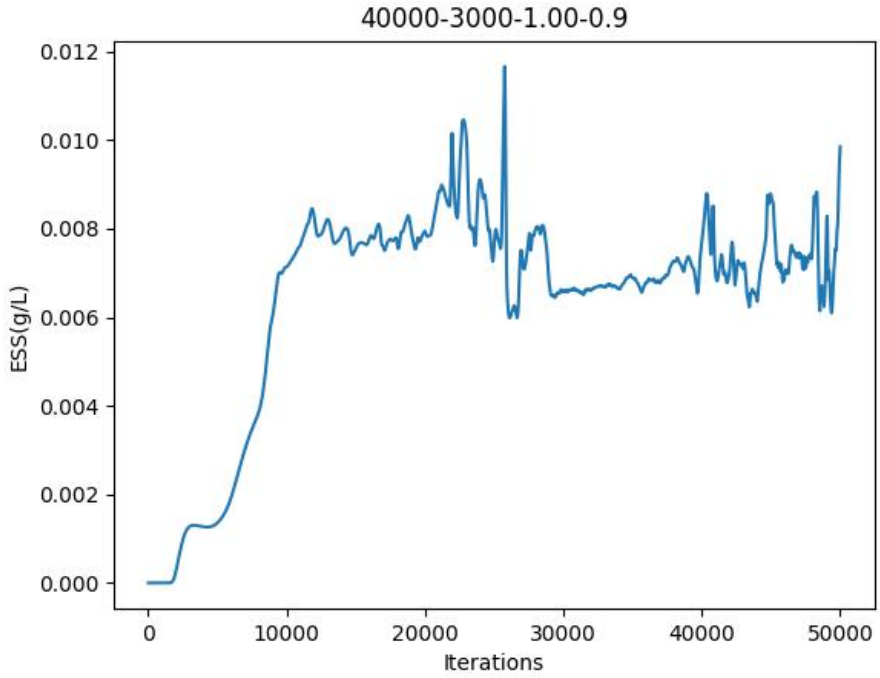
40000-3000-1.00-0.9
ESS(g/L)
0.000
0.002
0.004
0.006
0.008
0.010
0.012
0
10000
20000
30000
40000
50000
Iterations

7.2 Set C: ESS at SOR=781 gal/ft2/day

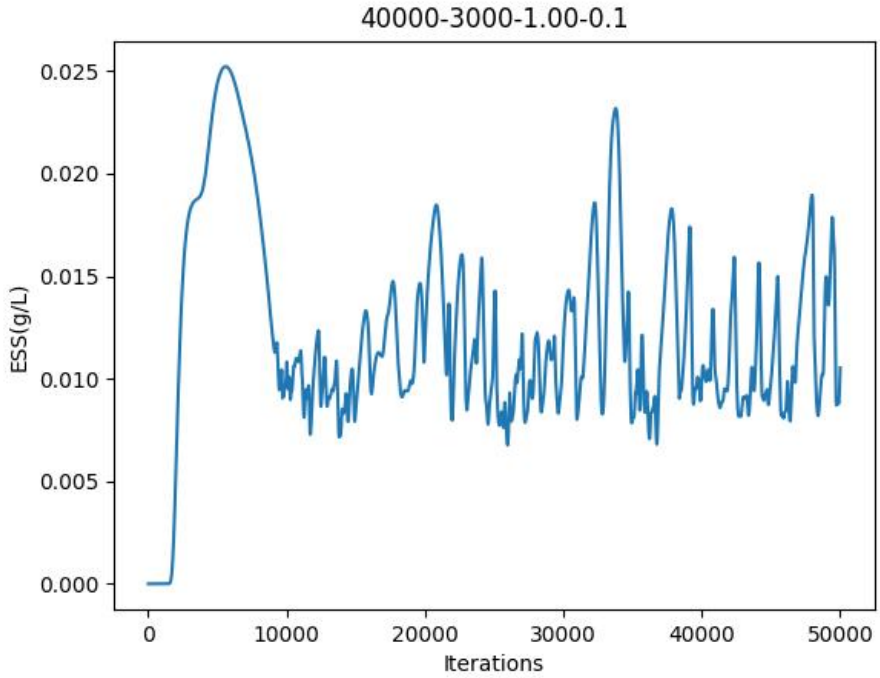

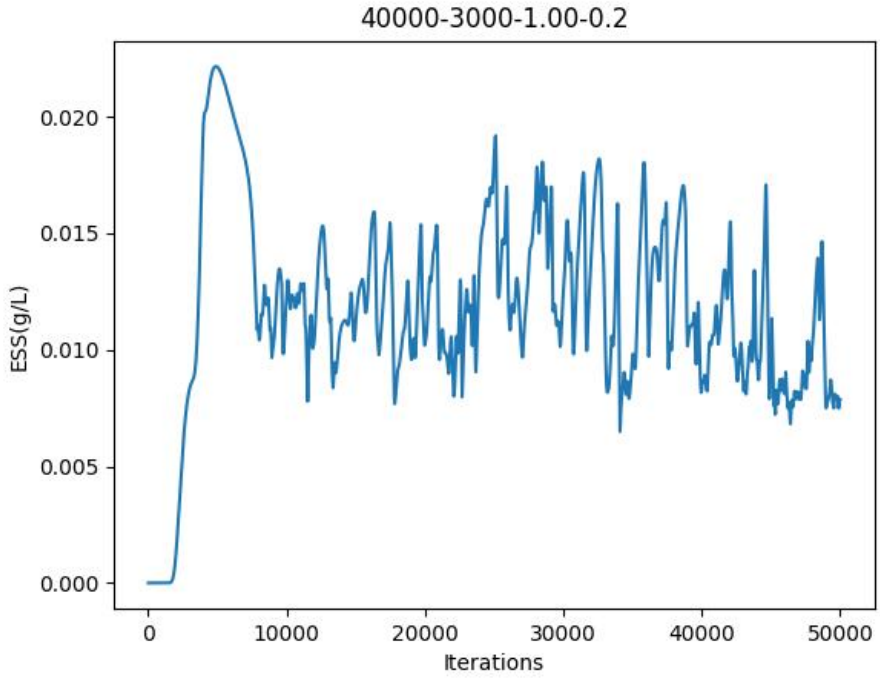

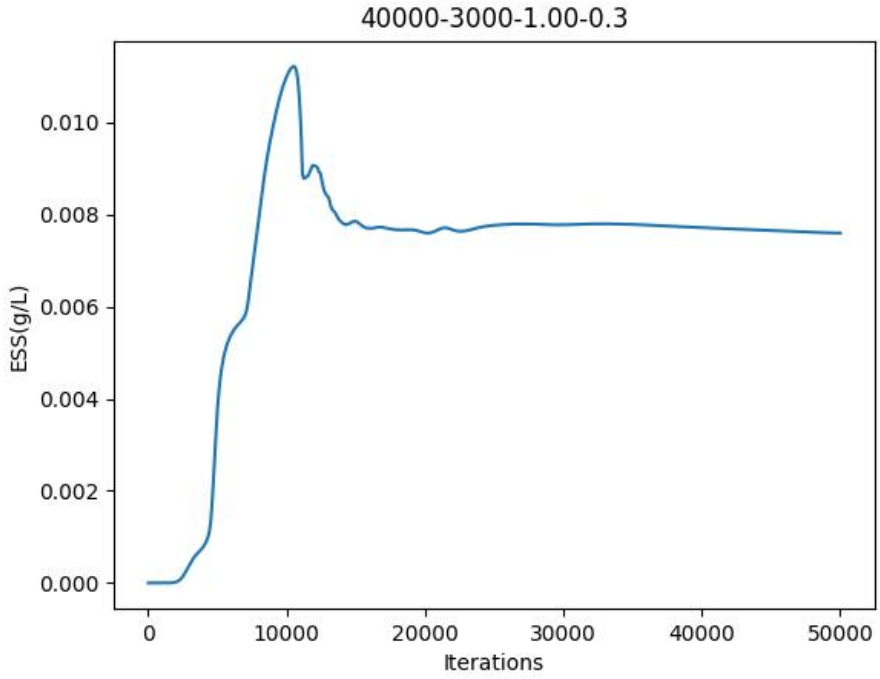
40000-3000-1.00-0.3
ESS(g/L)
0.010
0.008
0.006
0.004
0.002
0.000
0
10000
20000
30000
40000
50000
Iterations

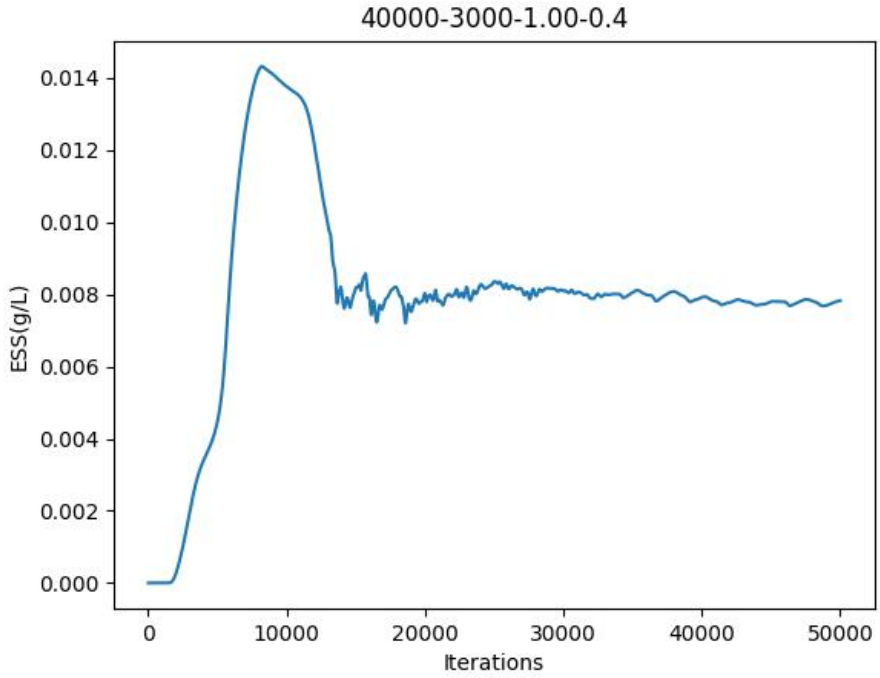
40000-3000-1.00-0.4
ESS(g/L)
0.014
0.012
0.010
0.008
0.006
0.004
0.002
0.000
0
10000
20000
30000
40000
50000
Iterations

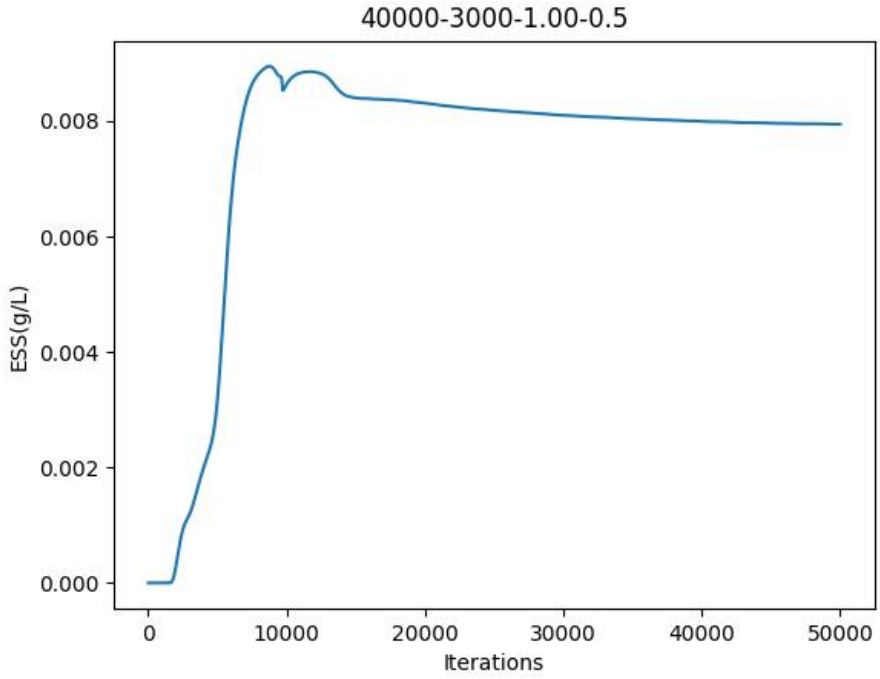
40000-3000-1.00-0.5
ESS(g/L)
0.000
0.002
0.004
0.006
0.008
0
10000
20000
30000
40000
50000
Iterations

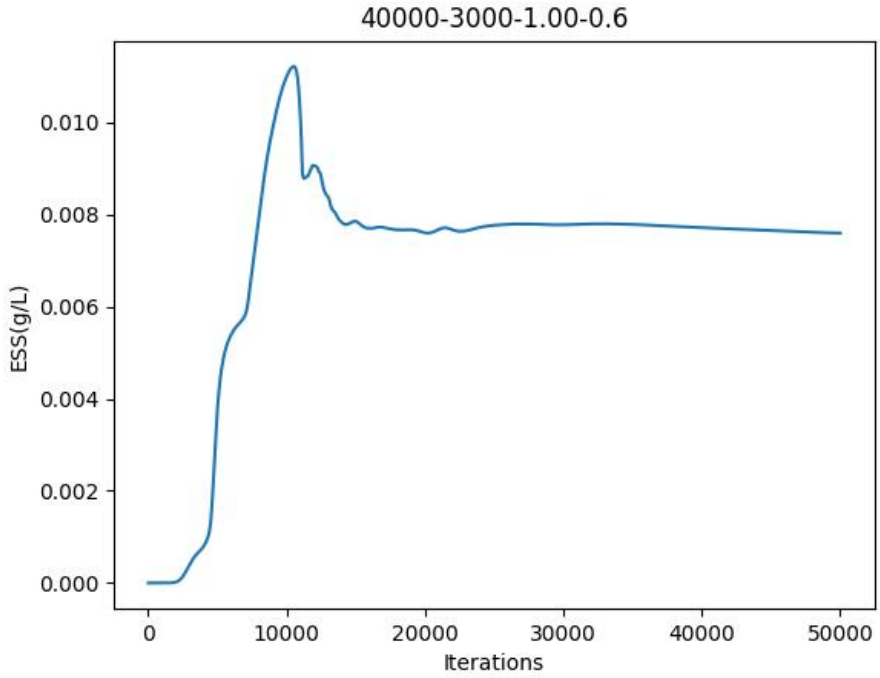
40000-3000-1.00-0.6
ESS(g/L)
0.000
0.002
0.004
0.006
0.008
0.010
0
10000
20000
30000
40000
50000
Iterations

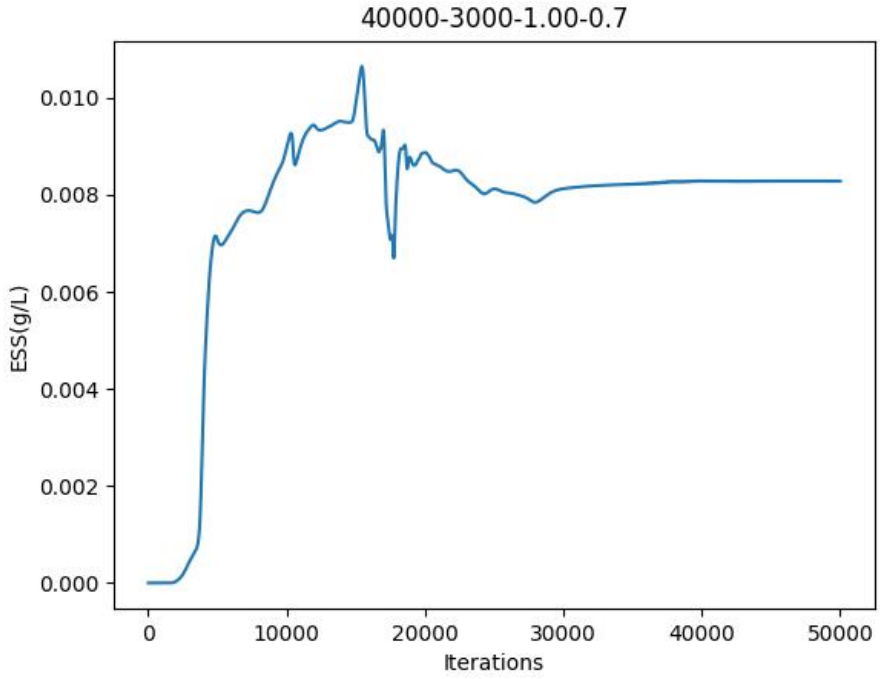
40000-3000-1.00-0.7
ESS(g/L)
0.010
0.008
0.006
0.004
0.002
0.000
0
10000
20000
30000
40000
50000
Iterations

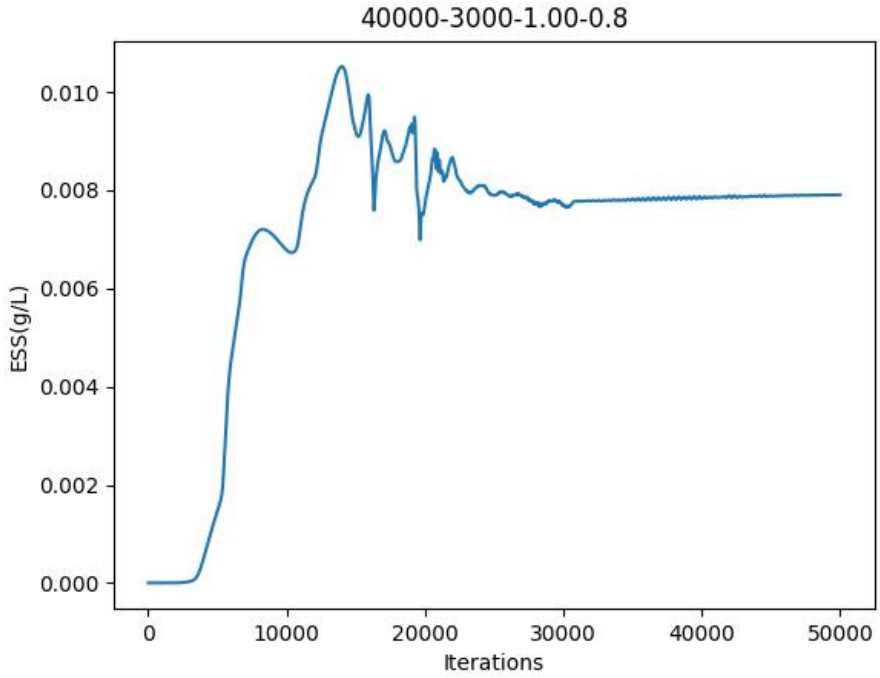
40000-3000-1.00-0.8
ESS(g/L)
0.010
0.008
0.006
0.004
0.002
0.000
0
10000
20000
30000
40000
50000
Iterations

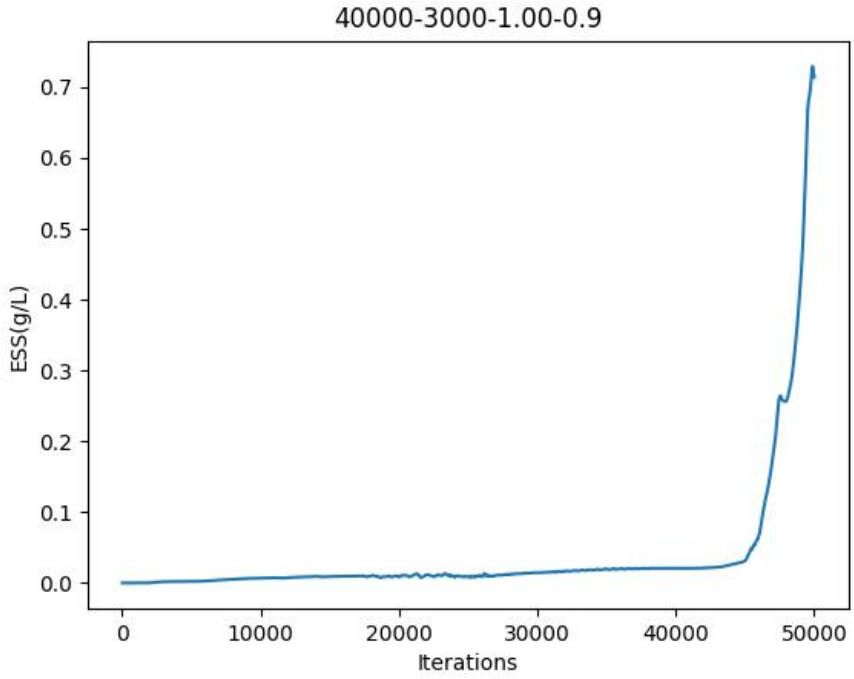

7.3 Set C: ESS at SOR=868 gal/ft2/day

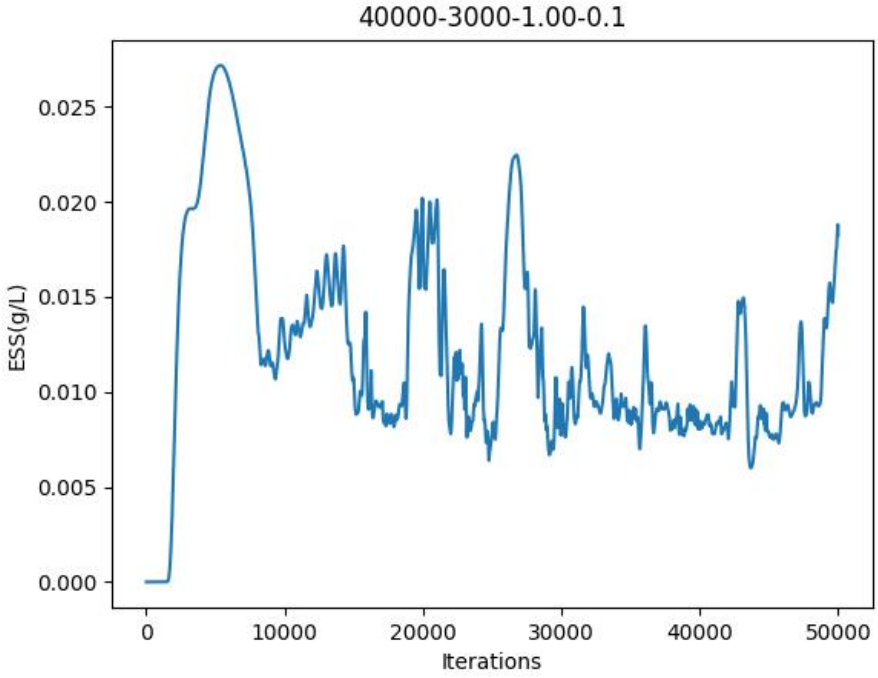

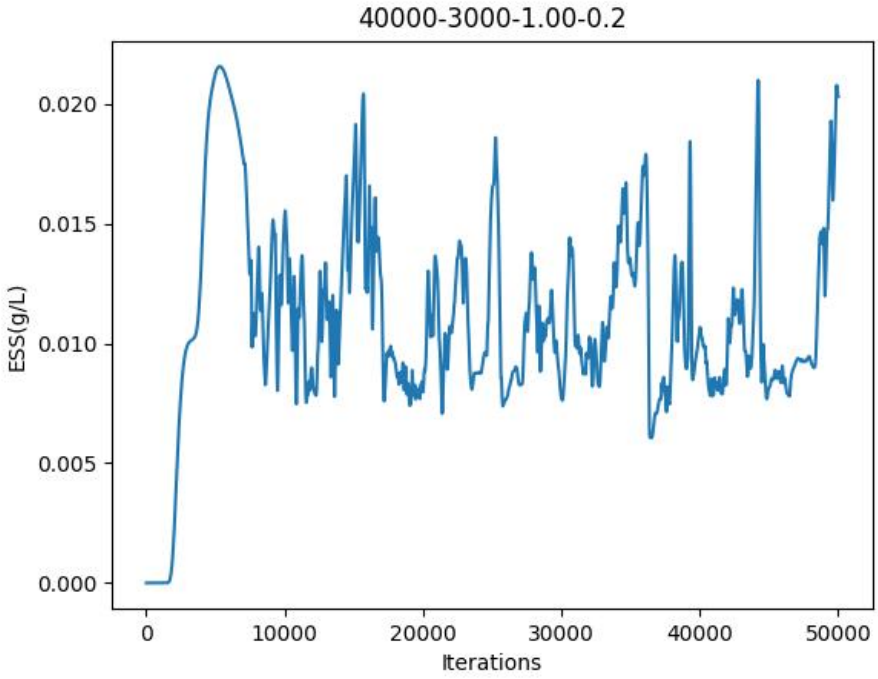
40000-3000-1.00-0.2
ESS(g/L)
0.020
0.015
0.010
0.005
0.000
0
10000
20000
30000
40000
50000
Iterations

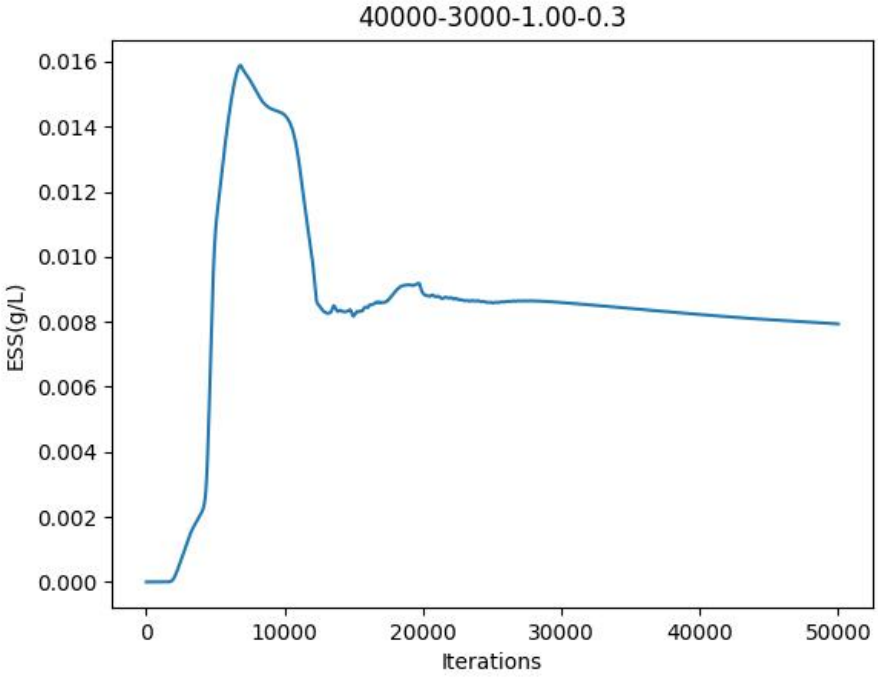
40000-3000-1.00-0.3
ESS(g/L)
0.016
0.014
0.012
0.010
0.008
0.006
0.004
0.002
0.000
0
10000
20000
30000
40000
50000
Iterations

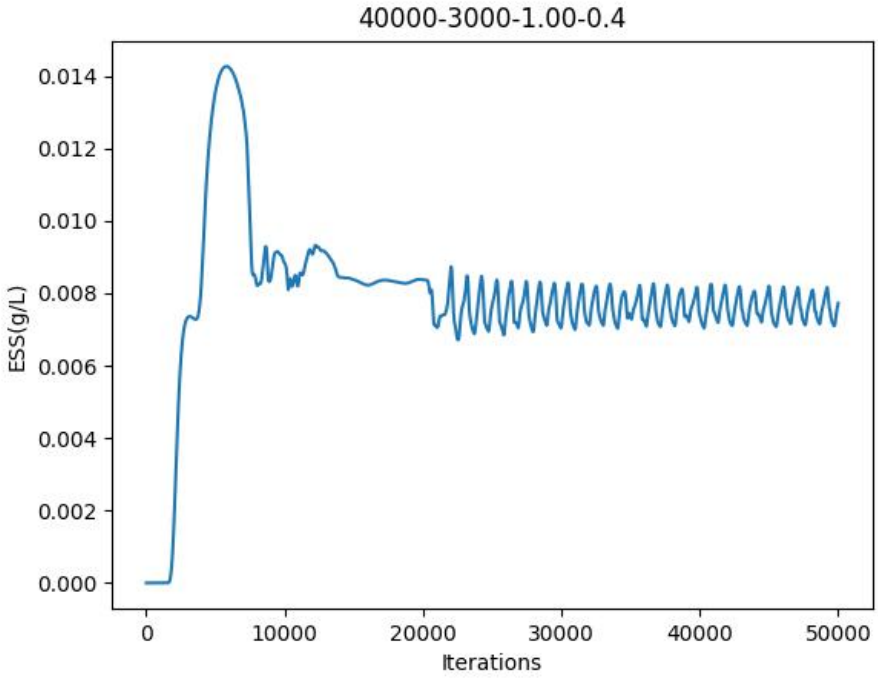
40000-3000-1.00-0.4
ESS(g/L)
0.014
0.012
0.010
0.008
0.006
0.004
0.002
0.000
0
10000
20000
30000
40000
50000
Iterations

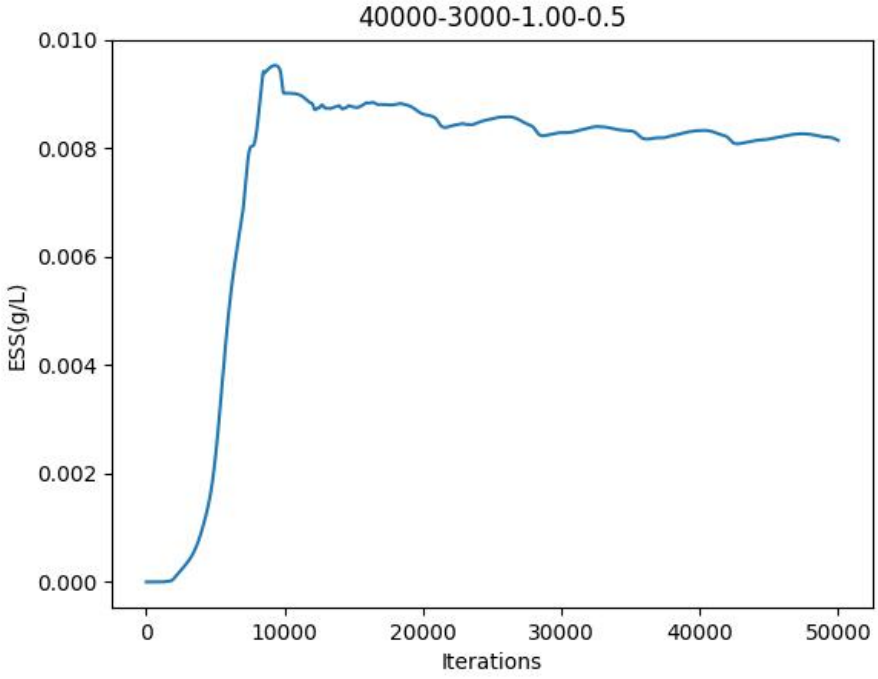
40000-3000-1.00-0.5
ESS(g/L)
0.010
0.008
0.006
0.004
0.002
0.000
0
10000
20000
30000
40000
50000
Iterations

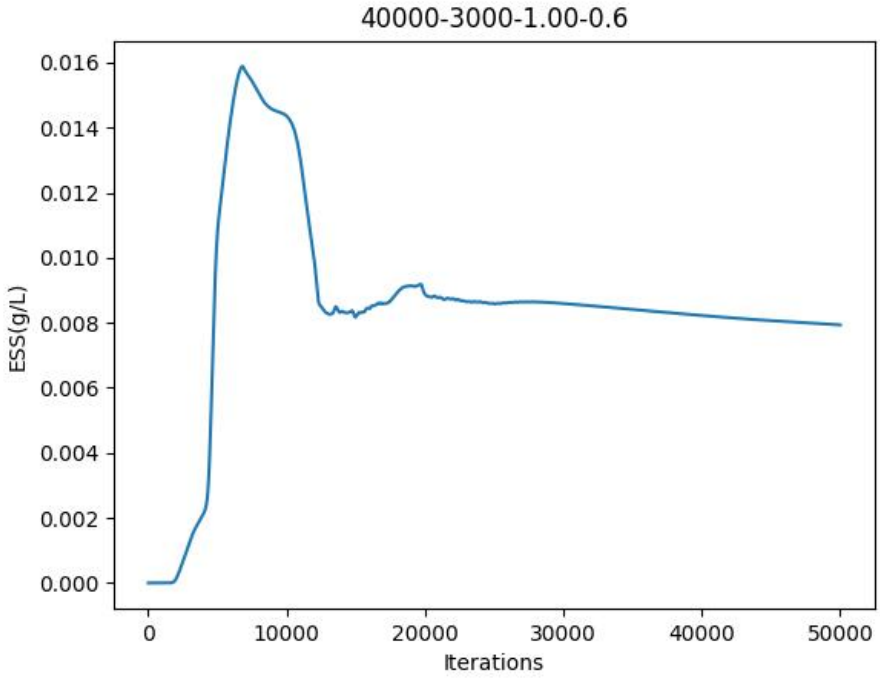
40000-3000-1.00-0.6
ESS(g/L)
0.016
0.014
0.012
0.010
0.008
0.006
0.004
0.002
0.000
0
10000
20000
30000
40000
50000
Iterations

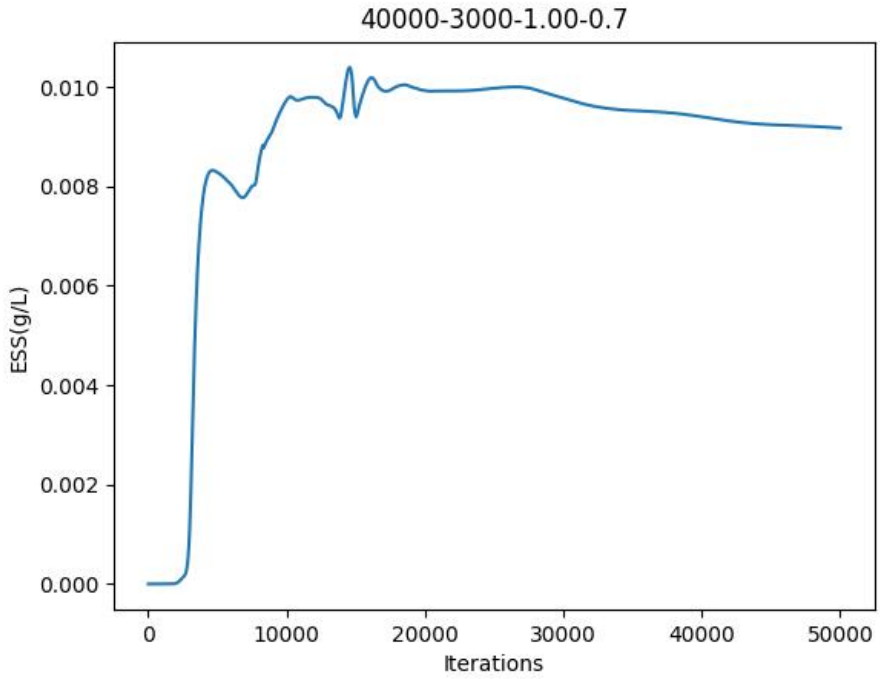
40000-3000-1.00-0.7
ESS(g/L)
0.010
0.008
0.006
0.004
0.002
0.000
0
10000
20000
30000
40000
50000
Iterations

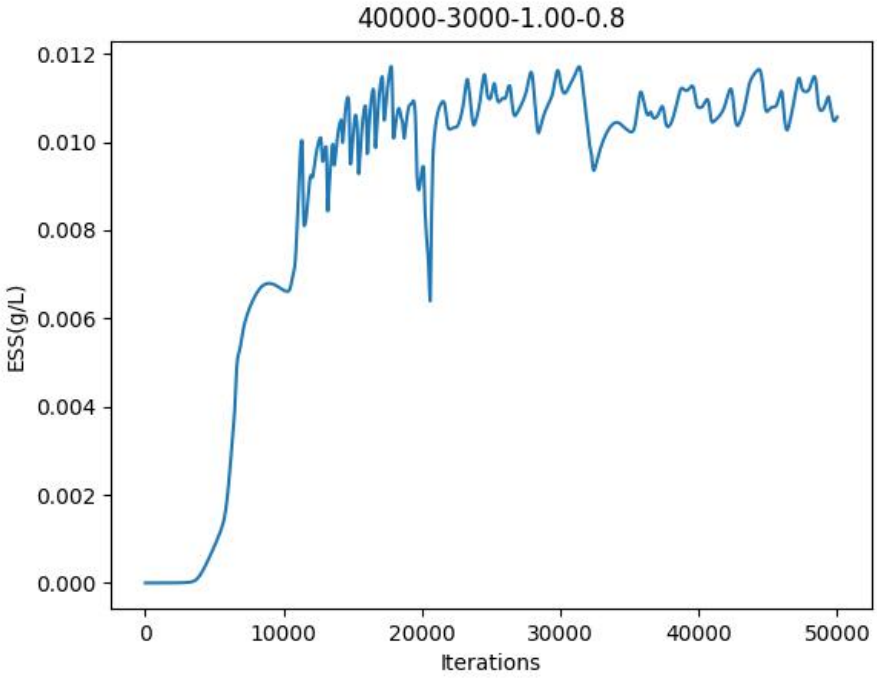
40000-3000-1.00-0.8
ESS(g/L)
0.012
0.010
0.008
0.006
0.004
0.002
0.000
0
10000
20000
30000
40000
50000
Iterations

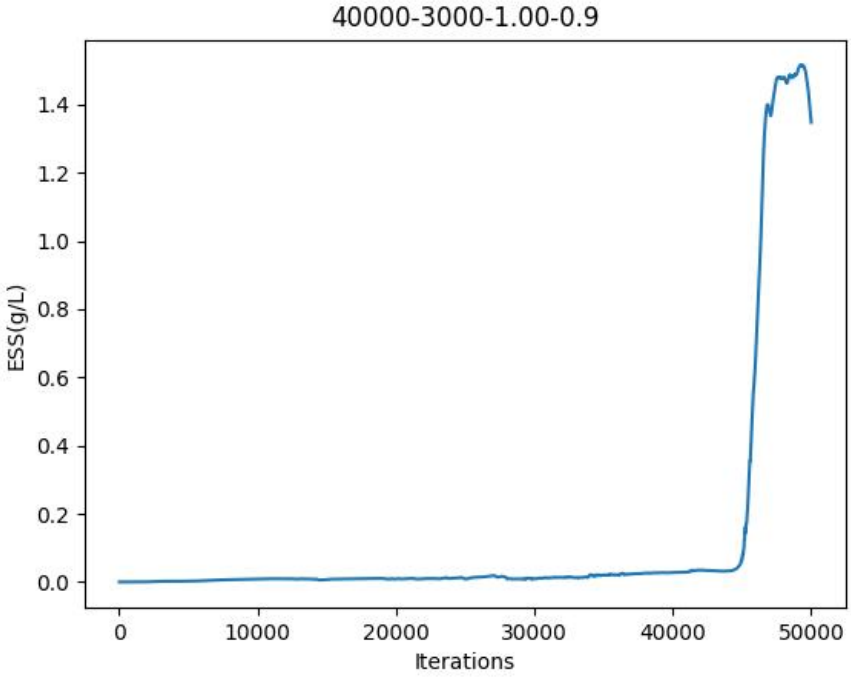
40000-3000-1.00-0.9
ESS(g/L)
1.4
1.2
1.0
0.8
0.6
0.4
0.2
0.0
0
10000
20000
30000
40000
50000
Iterations